Applied Mathematical Modelling 138 (2025) 115770

Contents lists available at ScienceDirect

Applied Mathematical Modelling

journal homepage: www.elsevier.com/locate/apm

Harmonic and superharmonic wave propagation in 2D mechanical metamaterials with inertia amplification

Marco Lepidi [a,*], Valeria Settimi [b]

[a] DICCA - Department of Civil, Chemical and Environmental Engineering, University of Genova, Genova, Italy
[b] DICEA - Department of Civil and Building Engineering, and Architecture, Polytechnic University of Marche, Ancona, Italy

ARTICLE INFO

Keywords:
Periodic materials
Nonlinear dynamics
Perturbation methods
Dispersion relation
Floppy modes
Superharmonic depolarization

ABSTRACT

An original parametric lattice model is proposed to investigate harmonic and superharmonic planar waves propagating in a two-dimensional mechanical metamaterial, whose periodic microstructure is characterized by local linkage mechanisms for pantographic inertia amplification. The free undamped dynamics in the metamaterial plane is governed by differential difference equations of motion, featuring geometric nonlinearities of both elastic and inertial nature. Within the weakly nonlinear oscillation regime, multi-harmonic wave solutions are achieved analytically, although asymptotically, by means of a suited perturbation method. At the lowest perturbation order, the linear dispersion properties (wavefrequencies and waveforms) of freely propagating monoharmonic waves are determined analytically as functions of the mechanical parameters. At higher perturbation orders, the amplitudes of the superharmonic wave components generated by quadratic and cubic nonlinearities are determined analytically, in the absence of internal resonances. Furthermore, the nonlinear corrections of the linear wavefrequencies are obtained. Smooth transitions from hardening to softening behaviors (or viceversa) are found to occur along particular propagation directions, depending on the wavelength. Physically, a pair of unexplored and interesting dynamic phenomena are disclosed. First, the free propagation of transversal waves along particular directions is characterized – independently of the wavenumber – by essentially nonlinear waveforms (*floppy modes*), featuring evanescent amplitude-dependent wavefrequency. Second, the generation of superharmonic components oscillating with double and triple frequency multiples – caused by quadratic and cubic nonlinearities – can determine a loss of polarization (*superharmonic depolarization*) in waves propagating with perfectly polarized waveforms in the linear field.

1. Introduction

Geometric and constitutive nonlinearities are known to significantly affect the spectral dispersion properties characterizing the propagation of harmonic waves in a variety of periodic microstructured media, ranging from granular chains to phononic crystals and mechanical metamaterials [1–5]. The macroscopical dynamic behavior of mechanical metamaterials, in particular, can be governed by properly designing the topology, compositeness and architecture of the periodic cellular microstructure. Indeed, microstructural properties can be optimized to achieve extraordinary or exotic performances, which are unattainable by natural or traditional syn-

* Corresponding author.
E-mail address: marco.lepidi@unige.it (M. Lepidi).

https://doi.org/10.1016/j.apm.2024.115770
Received 17 April 2024; Received in revised form 8 October 2024; Accepted 14 October 2024

Available online 18 October 2024

thetic materials [6–8]. Within this vibrating field of investigation, new possibilities are continuously being opened by the refinement of physical-mathematical formulations, the efficiency of new methodological tools, and the increment of available computational resources. Further impulse comes from recent disruptive developments in microengineering, high-precision manufacturing and high-fidelity prototyping.

Overcoming the classic concept of structural materials as averagely homogeneous media, bearing static loads and passively sustaining the propagation of bulk and shear waves, allows contemporary researchers to regard mechanical metamaterials as functional systems, which may work as smart vibration waveguides, broadband phononic filters, directional energy propagators, acoustic polarizers and rectifiers [9–12]. These functionalities result in fascinating engineering applications, including impact absorption, sound equalization, wave focusing, energy harvesting, vibration shielding and invisibility cloaking, among many others.

Within this stimulating and rapidly-developing framework, the endless search for groundbreaking solutions tends to continuously challenge the physical or technical limits of constituent materials and cellular microstructures. Consequently, nonlinear phenomena originated by high-amplitude oscillations may develop unexpectedly, when the operating field of innovative metamaterials is pushed beyond the linear range of infinitesimal strains or displacements. According to more ambitious strategies, nonlinear behaviors can also be pursued intentionally, typically by introducing auxiliary intracellular (local) mechanisms – like resonators, absorbers, inerters, pantographs, trampolines and sinks – whose performances are featured by highly or even essentially nonlinear properties. The leading idea is to take advantage of a variety of dynamic effects, including (i) amplitude-dependent spectral properties, with the amplitude serving as extra design variable, (ii) incremented spectral densities in the frequency band structure, due to subharmonic and superharmonic components, (iii) incipient dispersion in linearly nondispersive media, caused by the sensitivity of phase and group velocities to finite deformations, (iv) coexisting multiple branches of switchable stable solutions, originated by bifurcation onsets, (v) non-reciprocal targeted energy transfers, governed by resonance-driven interactions among stable and unstable nonlinear waveforms, (vi) self-reinforcing localized packets of solitary waves, sustained by a balanced cancellation of nonlinear and dispersive effects. The key to foster and harness these theoretical and methodological trends is the consistent treatment of the different and important nonlinearities that may arise from the high flexibilities, constitutive asymmetries, low dampings and amplified inertias characterizing the growing multiplicity of intracellular local mechanisms.

Based on this motivating background, the present paper is focused on the weakly nonlinear dynamics of two-dimensional mechanical metamaterials with inertia amplification. Conceptually, powerful local effects of inertial force amplification can be achieved by designing pantographic truss micromechanisms connecting eccentric masses [13–15]. Mechanically, the pantographic microstructural scheme grants a threefold advantage. Firstly, the rigidly-connected eccentric masses do not introduce additional active degrees-of-freedom and – consequently – do not enlarge the dimension of the dynamic model. Secondly, the pantographic mechanism, being kinematically indeterminate, does not increase the microstructural stiffness and, therefore, does not alter the quasistatic performance of the metamaterial. Lastly, the mechanical linkage of hinged rigid bodies required to build up the pantographic scheme is easily realizable from a technological viewpoint [16]. In the small-amplitude oscillation range, the linear dispersion properties of one-dimensional and two-dimensional metamaterials can be successfully designed for achieving desired spectral functionalities. Particularly, regulating the inertia amplification may effectively govern the opening or closing of low-frequency stop bands inhibiting the propagation of elastic waves [17–20]. In the large-amplitude oscillation range, important nonlinearities of inertial nature are generated by the local pantographic mechanisms in the equations governing the harmonic wave propagation. Particularly, the amplitude-dependent distortion of the linear dispersion properties (wavefrequencies and waveforms) caused by quadratic and cubic inertial nonlinearities can be analytically determined by means of perturbation methods in one-dimensional waveguides [21,22].

The present paper has the primary objective of introducing an original Lagrangian model describing the nonlinear dynamics of two-dimensional mechanical metamaterials with inertia amplification (Section 2). With respect to the existing literature, the main character of originality is the complete description of the inertial *and* elastic nonlinearities characterizing the governing equations of motion. Attention is focused on determining the dispersion properties of linear harmonic waves and – especially – nonlinear multi-harmonic waves that freely propagate in the metamaterial (Section 3). As peculiar methodological approach, the free propagation of nonlinear multi-harmonic waves is parametrically investigated by virtue of a perturbation scheme scaling the Fourier components of the equation solutions. The oscillation amplitudes of the superharmonic components, the nonlinear corrections of the linear wavefrequencies and the polarization properties of the nonlinear response are analytically determined. A rich nonlinear scenario of unprecedented dynamic phenomena is described in relation to linearly polarized solutions and kinematically undetermined shear waves. The multi-harmonic wave solutions are finally reconstructed (Section 4).

2. Mechanical metamaterial

The minimal mechanical metamaterial characterized by inertia amplification can be physically realized by assembling a two-dimensional infinitely periodic array of massive point particles, or *atoms*, interconnected by local pantographic mechanisms (Fig. 1a). Each pantographic mechanism is a rhombic tetra-atomic microstructure, in which a pair of adjacent particles in a row or column (*primary atoms*) are elastically coupled to each other and rigidly connected to a pair of eccentric particles (*secondary atoms*). Geometrically, the natural configuration at rest of all primary atoms defines a regular (spatially periodic) planar square lattice $\mathcal{Z}$, characterized by orthogonal primitive periodicity (column) vectors $\mathbf{a}_1$ and $\mathbf{a}_2$, with identical amplitude L (Fig. 1b). Consequently, each lattice point P_{ij} (or *site*) is univocally identified by the position vector $\mathbf{x}_{ij} = \mathbf{A}\mathbf{z}$, where the two-by-two periodicity matrix $\mathbf{A} = \left[\mathbf{a}_1, \mathbf{a}_2\right]$ collects columnwise the periodicity vectors, while the column *site vector* $\mathbf{z} = (i, j) \in \mathbb{Z}^2$ collects the integer indexes i and j.

The elastic coupling between each pair of primary atoms is described by a linear spring with stiffness K, causing attractive or repulsive interatomic forces. The rigid connections between the primary and secondary atoms are modeled by indeformable

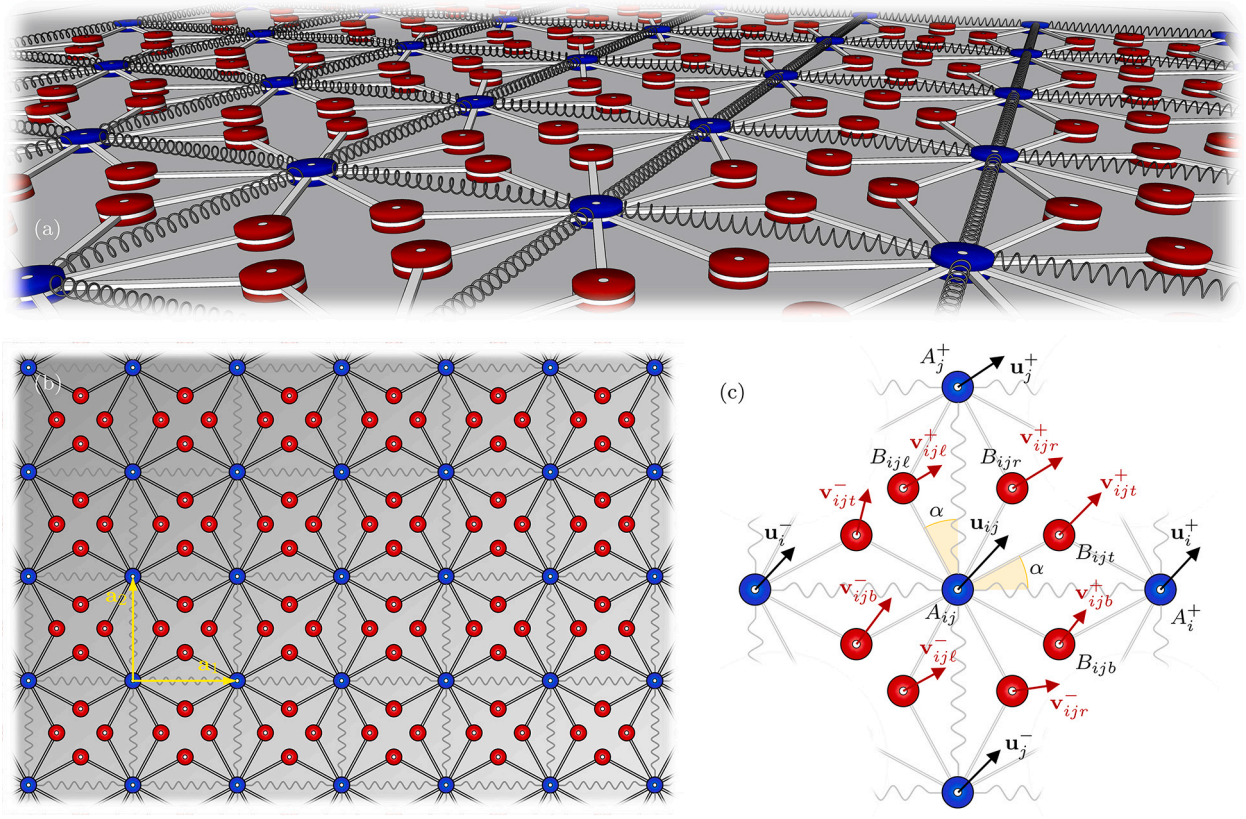

Fig. 1. Mechanical metamaterial with inertia amplification: (a) three-dimensional perspective view of the natural configuration, (b) two-dimensional periodic microstructure with distinction of primary (blue) atoms and secondary (red) atoms, (c) dynamic configuration described by planar displacement variables.

massless truss (hinged-hinged) elements, namely the *pantograph arms*. All the pantograph arms are inclined by the *pantographic angle* $\alpha \in (0, \pi/4)$ with respect to one or the other of the orthogonal array axes, which are collinear to the unitary vectors $\mathbf{n}_1 = \mathbf{a}_1/\|\mathbf{a}_1\|$ and $\mathbf{n}_2 = \mathbf{a}_2/\|\mathbf{a}_2\|$. The inertial masses of the primary and secondary atoms are denoted by M_p and M_s, respectively.

Taking the natural configuration at rest as a reference, all the primary and secondary atoms are allowed to develop only two-dimensional motions in the lattice plane. Consequently, the dynamic configuration of the generic primary atom A_{ij} located at the generic lattice point P_{ij} identified by the site vector $\mathbf{z} = (i, j)$ is described by the planar displacement vector $\mathbf{u}_{ij} = U_{ij}\mathbf{n}_1 + V_{ij}\mathbf{n}_2$ (Fig. 1c). The planar motion of the four secondary atoms B_{ijb}, B_{ijt}, $B_{ij\ell}$, B_{ijr}, pantographically connected to the reference primary atom and the two adjacent primary atoms A_i^+ and A_j^+ located at points P_i^+ and P_j^+ defined by the incremented site vectors $\mathbf{z}_i^+ = (i+1, j)$ and $\mathbf{z}_j^+ = (i, j+1)$, is described by the displacement vectors $\mathbf{v}_{ijk} = U_{ijk}\mathbf{n}_1 + V_{ijk}\mathbf{n}_2$ and $\mathbf{v}_{ijh} = U_{ijh}\mathbf{n}_1 + V_{ijh}\mathbf{n}_2$ (with $k = b, t$ and $h = \ell, r$). The indeformability conditions of the pantographic arms result in geometrically exact (trigonometric) relations $\mathbf{v}_{ijk} = \mathbf{f}_k(\mathbf{u}_{ij}, \mathbf{u}_i^+)$ and $\mathbf{v}_{ijh} = \mathbf{f}_h(\mathbf{u}_{ij}, \mathbf{u}_j^+)$, where $\mathbf{f}_k(\mathbf{u}_{ij}, \mathbf{u}_i^+)$ and $\mathbf{f}_h(\mathbf{u}_{ij}, \mathbf{u}_j^+)$ are non-commutative *constraining functions* and the convenient positions $\mathbf{u}_i^+ := \mathbf{u}_{(i+1)j}$ and $\mathbf{u}_j^+ := \mathbf{u}_{i(j+1)}$ are used to shorten the notation. These constrain relations impose that the motion of secondary atoms (slave variables) depend on the motion of primary atoms (master variables). Consequently, a suitable set of configurational Lagrangian coordinates of the mechanical model is composed by all (and only) the master variables $\mathbf{u}_{ij}$ for all $\mathbf{z} \in \mathbb{Z}^2$.

2.1. Fully nonlinear equations of motion

The dynamic equations of motion governing the free undamped oscillations of the two-dimensional metamaterial can be formulated by following the principles of Lagrangian mechanics. Specifically, the Lagrangian function $\mathcal{L} = \mathcal{T} - \mathcal{V}$ of the mechanical model can be introduced. According to an exact (non-infinitesimal) geometric description of the microstructural kinematics for the pantographic mechanisms and the linear springs, the kinetic energy $\mathcal{T}$ and the elastic potential energy $\mathcal{V}$ can be expressed as

$$\mathcal{T} = \frac{1}{2}\sum_{i,j}\left[M_p\dot{\mathbf{u}}_{ij}\cdot\dot{\mathbf{u}}_{ij} + M_s\sum_k \dot{\mathbf{v}}_{ijk}\cdot\dot{\mathbf{v}}_{ijk} + M_s\sum_h \dot{\mathbf{v}}_{ijh}\cdot\dot{\mathbf{v}}_{ijh}\right] \tag{1}$$

$$\mathcal{V} = \frac{1}{2}\sum_{i,j} K\left[\left[\left(L\mathbf{n}_1 + \mathbf{w}_i^+\right)\cdot\left(L\mathbf{n}_1 + \mathbf{w}_i^+\right)\right]^{\frac{1}{2}} - L\right]^2 + K\left[\left[\left(L\mathbf{n}_2 + \mathbf{w}_j^+\right)\cdot\left(L\mathbf{n}_2 + \mathbf{w}_j^+\right)\right]^{\frac{1}{2}} - L\right]^2 \tag{2}$$

where the differences $\mathbf{w}_i^+ = (\mathbf{u}_i^+ - \mathbf{u}_{ij})$ and $\mathbf{w}_j^+ = (\mathbf{u}_j^+ - \mathbf{u}_{ij})$ describe the relative displacements between the reference primary atom and the adjacent primary atoms at incremented positions. The geometric relations $\dot{\mathbf{v}}_{ijk} = \mathbf{F}_k\dot{\mathbf{u}}_{ij} + \mathbf{F}_{ik}^+\dot{\mathbf{u}}_i^+$ and $\dot{\mathbf{v}}_{ijh} = \mathbf{F}_h\dot{\mathbf{u}}_{ij} + \mathbf{F}_{jh}^+\dot{\mathbf{u}}_j^+$ can be employed to express the vector velocities $\dot{\mathbf{v}}_{ijk}$ and $\dot{\mathbf{v}}_{ijh}$ as functions of the Lagrangian velocities $\dot{\mathbf{u}}_{ij}$, $\dot{\mathbf{u}}_i^+$ and $\dot{\mathbf{u}}_j^+$, by introducing the velocity-independent Jacobians $\mathbf{F}_k(\mathbf{u}_{ij},\mathbf{u}_i^+) = \partial\mathbf{f}_k/\partial\mathbf{u}_{ij}$, $\mathbf{F}_{ik}^+(\mathbf{u}_{ij},\mathbf{u}_i^+) = \partial\mathbf{f}_k/\partial\mathbf{u}_i^+$, $\mathbf{F}_h(\mathbf{u}_{ij},\mathbf{u}_j^+) = \partial\mathbf{f}_h/\partial\mathbf{u}_{ij}$, $\mathbf{F}_{jh}^+(\mathbf{u}_{ij},\mathbf{u}_j^+) = \partial\mathbf{f}_h/\partial\mathbf{u}_j^+$.

By virtue of the lattice periodicity, the free dynamics can properly be studied by focusing on the generic primary atom A_{ij} located at the generic lattice site $\mathbf{z}$. Specifically, the exact fully-nonlinear (transcendental) Euler-Lagrange equations governing the free oscillations of the primary atom A_{ij} can be determined as

$$
\begin{aligned}
\frac{\mathrm{d}}{\mathrm{d}t}\left(\frac{\partial\mathcal{L}}{\partial\dot{\mathbf{u}}_{ij}}\right) - \frac{\partial\mathcal{L}}{\partial\mathbf{u}_{ij}} = {}& \Big(M_p\mathbf{I} + M_s\sum\nolimits_k(\mathbf{S}_k+\mathbf{R}_k) + M_s\sum\nolimits_h(\mathbf{S}_h+\mathbf{R}_h)\Big)\ddot{\mathbf{u}}_{ij} + \\
& + M_s\Big(\sum\nolimits_k(\dot{\mathbf{S}}_k+\dot{\mathbf{R}}_k) + M_s\sum\nolimits_h(\dot{\mathbf{S}}_h+\dot{\mathbf{R}}_h)\Big)\dot{\mathbf{u}}_{ij} + \\
& + M_s\sum\nolimits_k(\mathbf{S}_{ik}^+\ddot{\mathbf{u}}_i^+ + \mathbf{R}_{ik}^-\ddot{\mathbf{u}}_i^-) + M_s\sum\nolimits_h(\mathbf{S}_{jh}^+\ddot{\mathbf{u}}_j^+ + \mathbf{R}_{jh}^-\ddot{\mathbf{u}}_j^-) + \\
& + M_s\sum\nolimits_k(\dot{\mathbf{S}}_{ik}^+\dot{\mathbf{u}}_i^+ + \dot{\mathbf{R}}_{ik}^-\dot{\mathbf{u}}_i^-) + M_s\sum\nolimits_h(\dot{\mathbf{S}}_{jh}^+\dot{\mathbf{u}}_j^+ + \dot{\mathbf{R}}_{jh}^-\dot{\mathbf{u}}_j^-) + \\
& - \tfrac{1}{2}M_s\sum\nolimits_k\big[\mathbf{J}_k(\dot{\mathbf{u}}_{ij}\otimes\mathbf{I}) + 2\mathbf{J}_{ik}^+(\dot{\mathbf{u}}_i^+\otimes\mathbf{I})\big]\dot{\mathbf{u}}_{ij} - \tfrac{1}{2}M_s\sum\nolimits_k\mathbf{J}_{ik}^{\#}(\dot{\mathbf{u}}_i^+\otimes\mathbf{I})\dot{\mathbf{u}}_i^+ + \\
& - \tfrac{1}{2}M_s\sum\nolimits_h\big[\mathbf{J}_h(\dot{\mathbf{u}}_{ij}\otimes\mathbf{I}) + 2\mathbf{J}_{jh}^+(\dot{\mathbf{u}}_j^+\otimes\mathbf{I})\big]\dot{\mathbf{u}}_{ij} - \tfrac{1}{2}M_s\sum\nolimits_h\mathbf{J}_{jh}^{\#}(\dot{\mathbf{u}}_j^+\otimes\mathbf{I})\dot{\mathbf{u}}_j^+ + \\
& - \tfrac{1}{2}M_s\sum\nolimits_k\big[\mathbf{L}_k(\dot{\mathbf{u}}_{ij}\otimes\mathbf{I}) + 2\mathbf{L}_{ik}^-(\dot{\mathbf{u}}_i^-\otimes\mathbf{I})\big]\dot{\mathbf{u}}_{ij} - \tfrac{1}{2}M_s\sum\nolimits_k\mathbf{L}_{ik}^{=}(\dot{\mathbf{u}}_i^-\otimes\mathbf{I})\dot{\mathbf{u}}_i^- + \\
& - \tfrac{1}{2}M_s\sum\nolimits_h\big[\mathbf{L}_h(\dot{\mathbf{u}}_{ij}\otimes\mathbf{I}) + 2\mathbf{L}_{jh}^-(\dot{\mathbf{u}}_j^-\otimes\mathbf{I})\big]\dot{\mathbf{u}}_{ij} - \tfrac{1}{2}M_s\sum\nolimits_h\mathbf{L}_{jh}^{=}(\dot{\mathbf{u}}_j^-\otimes\mathbf{I})\dot{\mathbf{u}}_j^- + \\
& - \mathbf{K}_i^+\big(L\mathbf{n}_1+\mathbf{w}_i^+\big)\big[\big(L\mathbf{n}_1+\mathbf{w}_i^+\big)\cdot\big(L\mathbf{n}_1+\mathbf{w}_i^+\big)\big]^{-\frac{1}{2}}\Big[\big[\big(L\mathbf{n}_1+\mathbf{w}_i^+\big)\cdot\big(L\mathbf{n}_1+\mathbf{w}_i^+\big)\big]^{\frac{1}{2}} - L\Big] + \\
& - \mathbf{K}_j^+\big(L\mathbf{n}_2+\mathbf{w}_j^+\big)\big[\big(L\mathbf{n}_2+\mathbf{w}_j^+\big)\cdot\big(L\mathbf{n}_2+\mathbf{w}_j^+\big)\big]^{-\frac{1}{2}}\Big[\big[\big(L\mathbf{n}_2+\mathbf{w}_j^+\big)\cdot\big(L\mathbf{n}_2+\mathbf{w}_j^+\big)\big]^{\frac{1}{2}} - L\Big] + \\
& - \mathbf{K}_i^-\big(L\mathbf{n}_1+\mathbf{w}_i^-\big)\big[\big(L\mathbf{n}_1+\mathbf{w}_i^-\big)\cdot\big(L\mathbf{n}_1+\mathbf{w}_i^-\big)\big]^{-\frac{1}{2}}\Big[\big[\big(L\mathbf{n}_1+\mathbf{w}_i^-\big)\cdot\big(L\mathbf{n}_1+\mathbf{w}_i^-\big)\big]^{\frac{1}{2}} - L\Big] + \\
& - \mathbf{K}_j^-\big(L\mathbf{n}_2+\mathbf{w}_j^-\big)\big[\big(L\mathbf{n}_2+\mathbf{w}_j^-\big)\cdot\big(L\mathbf{n}_2+\mathbf{w}_j^-\big)\big]^{-\frac{1}{2}}\Big[\big[\big(L\mathbf{n}_2+\mathbf{w}_j^-\big)\cdot\big(L\mathbf{n}_2+\mathbf{w}_j^-\big)\big]^{\frac{1}{2}} - L\Big] = \mathbf{0}
\end{aligned}
\tag{3}
$$

where $\mathbf{I}$ is the two-by-two identity matrix and $\otimes$ indicates the Kronecker product. Since the mechanical model is infinitely periodic in the two-dimensional plane, the dynamic system (3) establishes a (countably) infinite set of vector equations in the unknowns $\mathbf{u}_{ij}$ (holding for each $\mathbf{z} = (i,j) \in \mathbb{Z}^2$) that does not require boundary conditions. From the mathematical viewpoint, the auxiliary displacement-dependent quantities

$$
\begin{aligned}
&\mathbf{S}_k(\mathbf{u}_{ij},\mathbf{u}_i^+) = \mathbf{F}_k^\top\mathbf{F}_k, && \mathbf{S}_{ik}^+(\mathbf{u}_{ij},\mathbf{u}_i^+) = (\mathbf{F}_{ik}^+)^\top\mathbf{F}_k, && \mathbf{S}_{ik}^{\#}(\mathbf{u}_{ij},\mathbf{u}_i^+) = (\mathbf{F}_{ik}^+)^\top\mathbf{F}_{ik}^+ \\
&\mathbf{S}_h(\mathbf{u}_{ij},\mathbf{u}_j^+) = \mathbf{F}_h^\top\mathbf{F}_h, && \mathbf{S}_{jh}^+(\mathbf{u}_{ij},\mathbf{u}_j^+) = (\mathbf{F}_{jh}^+)^\top\mathbf{F}_h, && \mathbf{S}_{jh}^{\#}(\mathbf{u}_{ij},\mathbf{u}_j^+) = (\mathbf{F}_{jh}^+)^\top\mathbf{F}_{jh}^+ \\
&\mathbf{R}_k(\mathbf{u}_{ij},\mathbf{u}_i^-) = \mathbf{G}_k^\top\mathbf{G}_k, && \mathbf{R}_{ik}^-(\mathbf{u}_{ij},\mathbf{u}_i^-) = (\mathbf{G}_{ik}^-)^\top\mathbf{G}_k, && \mathbf{R}_{ik}^{=}(\mathbf{u}_{ij},\mathbf{u}_i^-) = (\mathbf{G}_{ik}^-)^\top\mathbf{G}_{ik}^- \\
&\mathbf{R}_h(\mathbf{u}_{ij},\mathbf{u}_j^-) = \mathbf{G}_h^\top\mathbf{G}_h, && \mathbf{R}_{jh}^-(\mathbf{u}_{ij},\mathbf{u}_j^-) = (\mathbf{G}_{jh}^-)^\top\mathbf{G}_h, && \mathbf{R}_{jh}^{=}(\mathbf{u}_{ij},\mathbf{u}_j^-) = (\mathbf{G}_{jh}^-)^\top\mathbf{G}_{jh}^-
\end{aligned}
\tag{4}
$$

are used in the treatment of the kinetic energy. In equations (4) the Jacobians $\mathbf{G}_k(\mathbf{u}_{ij},\mathbf{u}_i^-) = \partial\mathbf{g}_k/\partial\mathbf{u}_{ij}$, $\mathbf{G}_{ik}^-(\mathbf{u}_{ij},\mathbf{u}_i^-) = \partial\mathbf{g}_k/\partial\mathbf{u}_i^-$, $\mathbf{G}_h(\mathbf{u}_{ij},\mathbf{u}_j^-) = \partial\mathbf{g}_h/\partial\mathbf{u}_{ij}$, $\mathbf{G}_{jh}^-(\mathbf{u}_{ij},\mathbf{u}_j^-) = \partial\mathbf{g}_h/\partial\mathbf{u}_j^-$ of the constraining functions $\mathbf{g}_k(\mathbf{u}_i^-,\mathbf{u}_{ij}) = \mathbf{f}_k(\mathbf{u}_i^-,\mathbf{u}_{ij})$ and $\mathbf{g}_h(\mathbf{u}_j^-,\mathbf{u}_{ij}) = \mathbf{f}_h(\mathbf{u}_j^-,\mathbf{u}_{ij})$ are also introduced, with convenient positions $\mathbf{u}_i^- := \mathbf{u}_{(i-1)j}$ and $\mathbf{u}_j^- := \mathbf{u}_{i(j-1)}$ to shorten the notation. The Jacobians (expressed in denominator layout)

$$
\begin{aligned}
&\mathbf{J}_k(\mathbf{u}_{ij},\mathbf{u}_i^+) = \frac{\partial\mathbf{s}_k}{\partial\mathbf{u}_{ij}}, && \mathbf{J}_h(\mathbf{u}_{ij},\mathbf{u}_j^+) = \frac{\partial\mathbf{s}_h}{\partial\mathbf{u}_{ij}}, && \mathbf{J}_{ik}^+(\mathbf{u}_{ij},\mathbf{u}_i^+) = \frac{\partial\mathbf{s}_{ik}^+}{\partial\mathbf{u}_{ij}} \\
&\mathbf{J}_{jh}^+(\mathbf{u}_{ij},\mathbf{u}_j^+) = \frac{\partial\mathbf{s}_{jh}^+}{\partial\mathbf{u}_{ij}}, && \mathbf{J}_{ik}^{\#}(\mathbf{u}_{ij},\mathbf{u}_i^+) = \frac{\partial\mathbf{s}_{ik}^{\#}}{\partial\mathbf{u}_{ij}}, && \mathbf{J}_{jh}^{\#}(\mathbf{u}_{ij},\mathbf{u}_j^+) = \frac{\partial\mathbf{s}_{jh}^{\#}}{\partial\mathbf{u}_{ij}} \\
&\mathbf{L}_k(\mathbf{u}_{ij},\mathbf{u}_i^-) = \frac{\partial\mathbf{r}_k}{\partial\mathbf{u}_{ij}}, && \mathbf{L}_h(\mathbf{u}_{ij},\mathbf{u}_j^-) = \frac{\partial\mathbf{r}_h}{\partial\mathbf{u}_{ij}}, && \mathbf{L}_{ik}^-(\mathbf{u}_{ij},\mathbf{u}_i^-) = \frac{\partial\mathbf{r}_{ik}^-}{\partial\mathbf{u}_{ij}} \\
&\mathbf{L}_{jh}^-(\mathbf{u}_{ij},\mathbf{u}_j^-) = \frac{\partial\mathbf{r}_{jh}^-}{\partial\mathbf{u}_{ij}}, && \mathbf{L}_{ik}^{=}(\mathbf{u}_{ij},\mathbf{u}_i^-) = \frac{\partial\mathbf{s}_{ik}^{=}}{\partial\mathbf{u}_{ij}}, && \mathbf{L}_{jh}^{=}(\mathbf{u}_{ij},\mathbf{u}_j^-) = \frac{\partial\mathbf{s}_{jh}^{=}}{\partial\mathbf{u}_{ij}}
\end{aligned}
\tag{5}
$$

of the matrix vectorializations $\mathbf{s}_k = \mathrm{vec}(\mathbf{S}_k)$, $\mathbf{s}_h = \mathrm{vec}(\mathbf{S}_h)$, $\mathbf{s}_{ik}^+ = \mathrm{vec}(\mathbf{S}_{ik}^+)$, $\mathbf{s}_{jh}^+ = \mathrm{vec}(\mathbf{S}_{jh}^+)$, $\mathbf{s}_{ik}^{\#} = \mathrm{vec}(\mathbf{S}_{ik}^{\#})$, $\mathbf{s}_{jh}^{\#} = \mathrm{vec}(\mathbf{S}_{jh}^{\#})$, $\mathbf{r}_k = \mathrm{vec}(\mathbf{R}_k)$, $\mathbf{r}_h = \mathrm{vec}(\mathbf{R}_h)$, $\mathbf{r}_{ik}^- = \mathrm{vec}(\mathbf{R}_{ik}^-)$, $\mathbf{r}_{jh}^- = \mathrm{vec}(\mathbf{R}_{jh}^-)$, $\mathbf{r}_{ik}^{=} = \mathrm{vec}(\mathbf{R}_{ik}^{=})$, $\mathbf{r}_{jh}^{=} = \mathrm{vec}(\mathbf{R}_{jh}^{=})$ are defined to employ the matrix form of the derivative of a matrix function with respect to a vector.

Finally, the Jacobians (expressed in denominator layout)

$$\mathbf{K}_i^+(\mathbf{u}_{ij},\mathbf{u}_i^+)=K\,\frac{\partial\left(L\mathbf{n}_1+\mathbf{w}_i^+\right)}{\partial\mathbf{u}_{ij}},\qquad \mathbf{K}_j^+(\mathbf{u}_{ij},\mathbf{u}_j^+)=K\,\frac{\partial\left(L\mathbf{n}_2+\mathbf{w}_j^+\right)}{\partial\mathbf{u}_{ij}}$$
$$\mathbf{K}_i^-(\mathbf{u}_{ij},\mathbf{u}_i^-)=K\,\frac{\partial\left(L\mathbf{n}_1+\mathbf{w}_i^-\right)}{\partial\mathbf{u}_{ij}},\qquad \mathbf{K}_j^-(\mathbf{u}_{ij},\mathbf{u}_j^-)=K\,\frac{\partial\left(L\mathbf{n}_2+\mathbf{w}_j^-\right)}{\partial\mathbf{u}_{ij}} \tag{6}$$

are introduced in the treatment of the potential elastic energy, together with the vector displacement differences $\mathbf{w}_i^-=(\mathbf{u}_{ij}-\mathbf{u}_i^-)$ and $\mathbf{w}_j^-=(\mathbf{u}_{ij}-\mathbf{u}_j^-)$. The indeformability conditions of the pantographic arms require valid solutions $\mathbf{u}_{ij}$ of equations (3) to respect the geometric inequalities on the relative displacements $\left(L\mathbf{n}_1+\mathbf{w}_i^+\right)\cdot\left(L\mathbf{n}_1+\mathbf{w}_i^+\right)<L^2\sec^2(\alpha)$ and $\left(L\mathbf{n}_2+\mathbf{w}_j^+\right)\cdot\left(L\mathbf{n}_2+\mathbf{w}_j^+\right)<L^2\sec^2(\alpha)$.

As complementary remark, it may be worth noting that the fully-nonlinear equations of motion (3) are expressed in a completely general form that systematically governs the free undamped dynamics of the entire large class of two-dimensional lattice materials characterized by kinetic and potential elastic energies mathematically expressible in the form (1)-(2).

2.2. Nonlinear equations of motion

The fully nonlinear equations of motion (3) can be conveniently expressed in nondimensional form. To this purpose, the known quantities L and $\Omega^2=K/M_p$ are selected as reference length and (square) frequency. Therefore, dimensionless variables and parameters are introduced

$$\tilde{\mathbf{u}}_{ij}=\frac{\mathbf{u}_{ij}}{L},\qquad \tilde{\mathbf{u}}_i^+=\frac{\mathbf{u}_i^+}{L},\qquad \tilde{\mathbf{u}}_i^-=\frac{\mathbf{u}_i^-}{L},\qquad \tilde{\mathbf{u}}_j^+=\frac{\mathbf{u}_j^+}{L},\qquad \tilde{\mathbf{u}}_j^-=\frac{\mathbf{u}_j^-}{L},\qquad \tau=\Omega t,\qquad \varrho^2=\frac{M_s}{M_p} \tag{7}$$

where the secondary-to-principal *mass ratio* ϱ^2 is strictly positive by definition. The mass ratio ϱ^2 and the amplification angle α represent the minimal set of independent dimensionless parameters sufficient to describe the geometric and mechanical properties of the metamaterial.

The fully-nonlinear equations of motion can be consistently approximated by expressing all the configuration variables in polynomial series, in the neighborhood of the rest configuration. Within the framework of small amplitude oscillations, only terms up to the third order can be retained. Consequently, the nonlinear (polynomial) equations of motion, expressed in matrix form, read

$$\begin{aligned}&\mathbf{M}_a\ddot{\mathbf{u}}_{ij}+\mathbf{M}_c(\ddot{\mathbf{u}}_i^-+\ddot{\mathbf{u}}_i^+)+\mathbf{M}_o(\ddot{\mathbf{u}}_j^-+\ddot{\mathbf{u}}_j^+)+2\mathbf{u}_{ij}+\mathbf{K}_c(\mathbf{u}_i^-+\mathbf{u}_i^+)+\mathbf{K}_o(\mathbf{u}_j^-+\mathbf{u}_j^+)+\\&\quad+\mathbf{k}_2(\mathbf{u}_{ij},\mathbf{u}_i^-,\mathbf{u}_i^+,\mathbf{u}_j^-,\mathbf{u}_j^+)+\mathbf{m}_2(\mathbf{u}_{ij},\mathbf{u}_i^-,\mathbf{u}_i^+,\mathbf{u}_j^-,\mathbf{u}_j^+,\dot{\mathbf{u}}_{ij},\dot{\mathbf{u}}_i^-,\dot{\mathbf{u}}_i^+,\dot{\mathbf{u}}_j^-,\dot{\mathbf{u}}_j^+,\ddot{\mathbf{u}}_{ij},\ddot{\mathbf{u}}_i^-,\ddot{\mathbf{u}}_i^+,\ddot{\mathbf{u}}_j^-,\ddot{\mathbf{u}}_j^+)+\\&\quad+\mathbf{k}_3(\mathbf{u}_{ij},\mathbf{u}_i^-,\mathbf{u}_i^+,\mathbf{u}_j^-,\mathbf{u}_j^+)+\mathbf{m}_3(\mathbf{u}_{ij},\mathbf{u}_i^-,\mathbf{u}_i^+,\mathbf{u}_j^-,\mathbf{u}_j^+,\dot{\mathbf{u}}_{ij},\dot{\mathbf{u}}_i^-,\dot{\mathbf{u}}_i^+,\dot{\mathbf{u}}_j^-,\dot{\mathbf{u}}_j^+,\ddot{\mathbf{u}}_{ij},\ddot{\mathbf{u}}_i^-,\ddot{\mathbf{u}}_i^+,\ddot{\mathbf{u}}_j^-,\ddot{\mathbf{u}}_j^+)=\mathbf{0}\end{aligned} \tag{8}$$

where the tilde has been omitted for the sake of simplicity and the dot indicates differentiation with respect to dimensionless time τ. The two-by-two mass matrices are $\mathbf{M}_a=\varrho_a^2\mathbf{I}$, $\mathbf{M}_c=\mathrm{diag}(\varrho_c^2,\varrho_o^2)$, $\mathbf{M}_o=\mathrm{diag}(\varrho_o^2,\varrho_c^2)$, while the two-by-two stiffness matrices are $\mathbf{K}_c=\mathbf{E}_{11}$, $\mathbf{K}_o=\mathbf{E}_{22}$, with $\mathbf{E}_{ij}$ indicating the single-entry matrix.

By introducing the components of the nonlinearity vectors $\mathbf{k}_2=(\kappa_2^u,\kappa_2^v)$, $\mathbf{k}_3=(\kappa_3^u,\kappa_3^v)$ – depending on the displacements only – and $\mathbf{m}_2=(\mu_2^u,\mu_2^v)$, $\mathbf{m}_3=(\mu_3^u,\mu_3^v)$ – depending on displacements, velocities and accelerations – the governing equation can be expressed in component form

$$\begin{aligned}&\varrho_a^2\ddot{u}_{ij}+\varrho_c^2(\ddot{u}_i^-+\ddot{u}_i^+)+\varrho_o^2(\ddot{u}_j^-+\ddot{u}_j^+)+(2u_{ij}-u_i^--u_i^+)+\\&\quad+\kappa_2^u(\mathbf{u}_{ij},\mathbf{u}_i^-,\mathbf{u}_i^+,\mathbf{u}_j^-,\mathbf{u}_j^+)+\mu_2^u(\mathbf{u}_{ij},\mathbf{u}_i^-,\mathbf{u}_i^+,\mathbf{u}_j^-,\mathbf{u}_j^+,\dot{\mathbf{u}}_{ij},\dot{\mathbf{u}}_i^-,\dot{\mathbf{u}}_i^+,\dot{\mathbf{u}}_j^-,\dot{\mathbf{u}}_j^+,\ddot{\mathbf{u}}_{ij},\ddot{\mathbf{u}}_i^-,\ddot{\mathbf{u}}_i^+,\ddot{\mathbf{u}}_j^-,\ddot{\mathbf{u}}_j^+)+\\&\quad+\kappa_3^u(\mathbf{u}_{ij},\mathbf{u}_i^-,\mathbf{u}_i^+,\mathbf{u}_j^-,\mathbf{u}_j^+)+\mu_3^u(\mathbf{u}_{ij},\mathbf{u}_i^-,\mathbf{u}_i^+,\mathbf{u}_j^-,\mathbf{u}_j^+,\dot{\mathbf{u}}_{ij},\dot{\mathbf{u}}_i^-,\dot{\mathbf{u}}_i^+,\dot{\mathbf{u}}_j^-,\dot{\mathbf{u}}_j^+,\ddot{\mathbf{u}}_{ij},\ddot{\mathbf{u}}_i^-,\ddot{\mathbf{u}}_i^+,\ddot{\mathbf{u}}_j^-,\ddot{\mathbf{u}}_j^+)=0\end{aligned} \tag{9}$$

$$\begin{aligned}&\varrho_a^2\ddot{v}_{ij}+\varrho_c^2(\ddot{v}_j^-+\ddot{v}_j^+)+\varrho_o^2(\ddot{v}_i^-+\ddot{v}_i^+)+(2v_{ij}-v_j^--v_j^+)+\\&\quad+\kappa_2^v(\mathbf{u}_{ij},\mathbf{u}_i^-,\mathbf{u}_i^+,\mathbf{u}_j^-,\mathbf{u}_j^+)+\mu_2^v(\mathbf{u}_{ij},\mathbf{u}_i^-,\mathbf{u}_i^+,\mathbf{u}_j^-,\mathbf{u}_j^+,\dot{\mathbf{u}}_{ij},\dot{\mathbf{u}}_i^-,\dot{\mathbf{u}}_i^+,\dot{\mathbf{u}}_j^-,\dot{\mathbf{u}}_j^+,\ddot{\mathbf{u}}_{ij},\ddot{\mathbf{u}}_i^-,\ddot{\mathbf{u}}_i^+,\ddot{\mathbf{u}}_j^-,\ddot{\mathbf{u}}_j^+)+\\&\quad+\kappa_3^v(\mathbf{u}_{ij},\mathbf{u}_i^-,\mathbf{u}_i^+,\mathbf{u}_j^-,\mathbf{u}_j^+)+\mu_3^v(\mathbf{u}_{ij},\mathbf{u}_i^-,\mathbf{u}_i^+,\mathbf{u}_j^-,\mathbf{u}_j^+,\dot{\mathbf{u}}_{ij},\dot{\mathbf{u}}_i^-,\dot{\mathbf{u}}_i^+,\dot{\mathbf{u}}_j^-,\dot{\mathbf{u}}_j^+,\ddot{\mathbf{u}}_{ij},\ddot{\mathbf{u}}_i^-,\ddot{\mathbf{u}}_i^+,\ddot{\mathbf{u}}_j^-,\ddot{\mathbf{u}}_j^+)=0\end{aligned} \tag{10}$$

where the (α,ϱ^2)-dependent quantities $\varrho_a^2=1+4\varrho^2\csc^2(2\alpha)$, $\varrho_c^2=\frac{1}{2}\varrho^2\left(1-\cot^2(\alpha)\right)$, $\varrho_o^2=\frac{1}{2}\varrho^2\cos(2\alpha)\sec^2(\alpha)$ can be recognized as linear coefficients of inertia amplification.

From the mathematical viewpoint, the governing equations (9) and (10) can be recognized as second-order ordinary differential (in time) second-order difference (in two-dimensional space) nonlinear homogeneous equations with constant coefficients. The two equations are formally identical (under proper interchange of the configuration variables), by virtue of the 4-order rotational symmetry of the mechanical model. Furthermore, the equations are linearly uncoupled, as expected, but nonlinearly coupled by quadratic and cubic nonlinearities, which can be recognized to have either inertial or elastic nature. The quadratic elastic terms (κ_2^u and κ_2^v) and the cubic elastic terms (κ_3^u and κ_3^v) are reported in the Appendix A.1, while the quadratic inertial terms (μ_2^u and μ_2^v) and the cubic inertial terms (μ_3^u and μ_3^v) are reported in the Appendix A.2. It may be worth remarking that the elastic nonlinearities are a peculiarity of the two-dimensional metamaterial, in which the primary atoms may develop a two degrees-of-freedom planar motion. On the contrary, quadratic and cubic nonlinearities of one-dimensional mechanical metamaterials with inertia amplifications have inertial nature only [21].

3. Wave propagation

In the absence of closed-form solutions and within the range of small-amplitude oscillations, perturbation methods are powerful and efficient tools to achieve analytical solutions, suited to asymptotically approximate exact solutions up to the desired level of accuracy. Specifically, perturbation techniques like the method of ordered Harmonic Balance [23,24], the Lindstedt-Poincaré method [25–28] the Multiple Scales method [21,29–33] and the Hamiltonian perturbation theory [34,35] have been successfully exploited in the field of mechanical metamaterials to disclose and describe interesting dynamic phenomena, like dispersion modulations, superharmonic frequency generations, enhanced dissipations, non-reciprocal energy transfers, supertransmission channels, oscillatory spatial modulation or saturating modulation at linear-nonlinear interfaces, solitary wave propagations and interactions.

To the purpose of the present work, the ordered Harmonic Balance method is employed and conveniently adapted to seek for a family of real-valued multi-harmonic wave solutions $\mathbf{u}_{ij}(\tau)=\mathbf{u}(\mathbf{z},\tau)$, which can be expressed in form of the two-dimensional exponential Fourier series

$$\mathbf{u}(\mathbf{z},\tau)=\mathbf{a}_0+\sum_{n=1}^{\infty}\epsilon^n\left(\mathbf{a}_n+\imath\,\mathbf{b}_n\right)\mathrm{e}^{-\imath\,(\boldsymbol{\beta}\cdot\mathbf{z}+n\omega\tau)}+\sum_{n=1}^{\infty}\epsilon^n\left(\mathbf{a}_n-\imath\,\mathbf{b}_n\right)\mathrm{e}^{\imath\,(\boldsymbol{\beta}\cdot\mathbf{z}+n\omega\tau)} \tag{11}$$

where $\imath$ is the imaginary unit. The real-valued variables $\mathbf{a}_n=(a_n,c_n)$ and $\mathbf{b}_n=(b_n,d_n)$ are the coefficients or *amplitudes* of the n-th Fourier series component. The solution describes periodic planar waves oscillating – in time – with dimensionless wavefrequency ω (*leading* harmonic component) and its integer multiples $n\omega$ (superharmonic components), while propagating – in space – through the two-dimensional lattice $\mathcal{Z}$, spanned by the integer position vector $\mathbf{z}=(i,j)\in\mathbb{Z}^2$, with real-valued dimensionless wavevector $\boldsymbol{\beta}=(\beta_1,\beta_2)\in\mathbb{R}^2$.

According to a standard perturbation scheme, the amplitudes $\mathbf{a}_n$ and $\mathbf{b}_n$ of the n-th Fourier component oscillating harmonically with wavefrequency $n\omega$, are ordered in integer n-power series of the small parameter $\epsilon\ll 1$, which plays a mere bookkeeping role. From the methodological viewpoint, this particular ordering of smallness postulates a priori that the amplitudes $\mathbf{a}_1$ (of the harmonic ω component), $\mathbf{a}_2,\mathbf{a}_3,\ldots,\mathbf{a}_n$ (of the superharmonic $2\omega,3\omega,\ldots,n\omega$ components) are smaller that the quasistatic amplitude $\mathbf{a}_0$ by one, two, three, ..., n powers of ϵ. Accordingly, the contribution of high harmonics becomes smaller and smaller for growing n, thus justifying the truncation of the Fourier series (at a finite number m of terms) on a physical ground.

By substituting solution (11) for $m=3$ into equation (8), expanding and collecting terms of the same ϵ-order, an ordered hierarchy of algebraic *perturbation equations* in the amplitude vectors $\mathbf{a}_n$ and $\mathbf{b}_n$ is carried out ($n=1,2,3$). Specifically, the n-th order states a linear complex-valued problem, which can be decomposed into a pair of independent, coupled equations in the unknown amplitudes $\mathbf{a}_n,\mathbf{b}_n$ by separating the real and imaginary parts. By virtue of the problem linearity, the solution – if determinable – is unique and generally depends on the solutions of all the lower order problems. Accordingly, the lowest order rules the linear wave dynamics of the system, which is found to be participated only by the first harmonic ω component (unknown amplitudes $\mathbf{a}_1$ and $\mathbf{b}_1$ of the leading harmonic component). The higher orders govern the nonlinear wave dynamics, which is found to be participated *also* by the superharmonic $2\omega,3\omega$ components (unknown amplitudes $\mathbf{a}_2,\mathbf{b}_2,\mathbf{a}_3,\mathbf{b}_3$). It may be noted that the quasistatic term (constant shift with amplitude $\mathbf{a}_0$) remains undetermined and is unessential for the analysis of the wave propagation.

Based on the above considerations, the quasistatic term $\mathbf{a}_0$ will be considered null in the following, for the sake of simplicity. Furthermore, the amplitude vectors $\mathbf{a}_1$ and $\mathbf{b}_1$ of the leading Fourier ω-component and the amplitude vectors $\mathbf{a}_n$ and $\mathbf{b}_n$ of the Fourier $n\omega$-component will be referred to as (*leading*) *harmonic amplitudes* and n-th *superharmonic amplitudes*, respectively, to simplify the nomenclature.

3.1. Linear dynamics

Focusing first on the lowest significant order ($n=1$), the perturbation equations state a pair of identical uncoupled eigenproblems that can be expressed in the form $\mathbf{H}(\omega,\boldsymbol{\beta})\,\mathbf{a}_1=\mathbf{0}$ and $\mathbf{H}(\omega,\boldsymbol{\beta})\,\mathbf{b}_1=\mathbf{0}$. Consequently, the unknown amplitudes $\mathbf{a}_1$ and $\mathbf{b}_1$ can be non trivial – although undetermined – if and only if the two-by-two coefficient matrix $\mathbf{H}(\omega,\boldsymbol{\beta})$ is singular. Since the matrix is diagonal by virtue of the linear uncoupling of the governing equations, its determinant is fully factorizable. Therefore, the characteristic equation imposing the singularity condition reads $F_a(\omega,\boldsymbol{\beta})F_c(\omega,\boldsymbol{\beta})=0$. By selecting the (square) wavefrequency ω^2 as unknown and the wavevector $\boldsymbol{\beta}$ as parameter, the solution of each eigenproblem counts two simple eigenvalues

$$\omega_a^2(\boldsymbol{\beta})=\frac{2(1-\cos\beta_1)}{1+\varrho^2\left[2(\cos\beta_1+\cos\beta_2)+(1-\cos\beta_1)\csc^2(\alpha)+(1-\cos\beta_2)\sec^2(\alpha)\right]} \tag{12}$$

$$\omega_c^2(\boldsymbol{\beta})=\frac{2(1-\cos\beta_2)}{1+\varrho^2\left[2(\cos\beta_2+\cos\beta_1)+(1-\cos\beta_2)\csc^2(\alpha)+(1-\cos\beta_1)\sec^2(\alpha)\right]} \tag{13}$$

with unitary algebraic and geometric multiplicity. The corresponding eigenvectors, describing the linear waveforms of the harmonic waves, coincide with the canonical vectors $\boldsymbol{\phi}_a=(1,0)$ and $\boldsymbol{\phi}_c=(0,1)$. Consequently, the linear free dynamics can be studied as superposition of two perfectly polarized waves. Indeed, in analogy with electromagnetic (linear) polarization and mechanical (modal) localization, an elastic wave can be considered perfectly polarized if its waveform is contributed by a single degree-of-freedom [36]. Accordingly, perfectly polarized waves of *longitudinal* (pressure) or *transverse* (shear) nature may occur only if the propagation direction (identified by the wavevector) is collinear with one or the other periodicity vector of the lattice. Along all the other directions, *mixed* (shear-pressure) waves propagate.

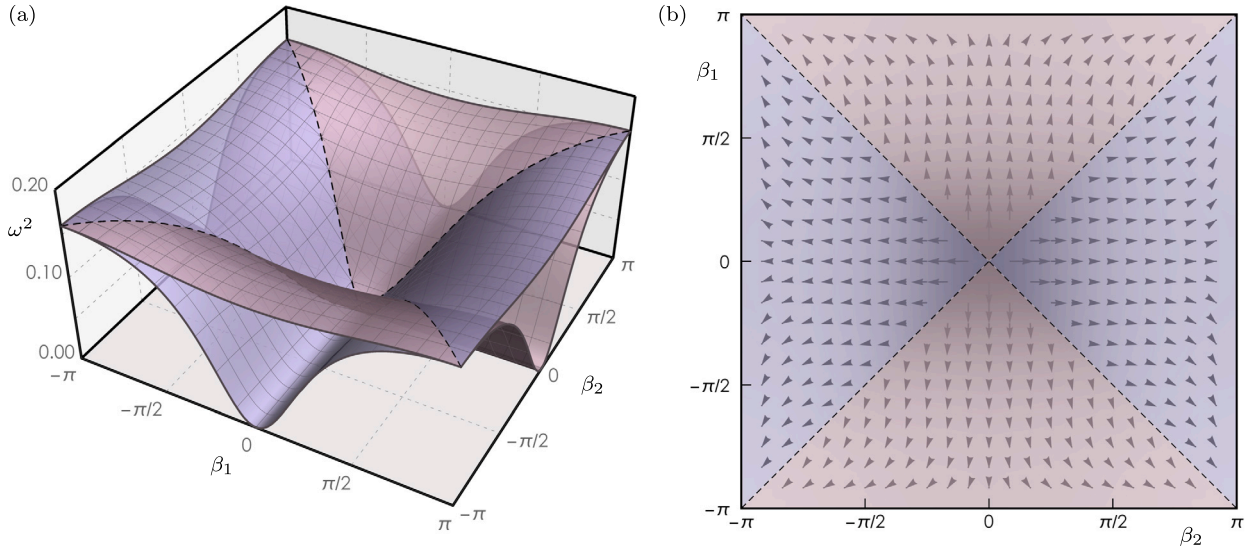

Fig. 2. Linear spectral properties of the mechanical metamaterial (for mass ratio $\varrho^2 = 2$ and amplification angle $\alpha = \pi/8$): (a) dispersion surfaces $\mathcal{S}_a$ (pink) and $\mathcal{S}_c$ (purple), (b) vector field of the group velocities $\mathbf{c}_a$ and $\mathbf{c}_c$.

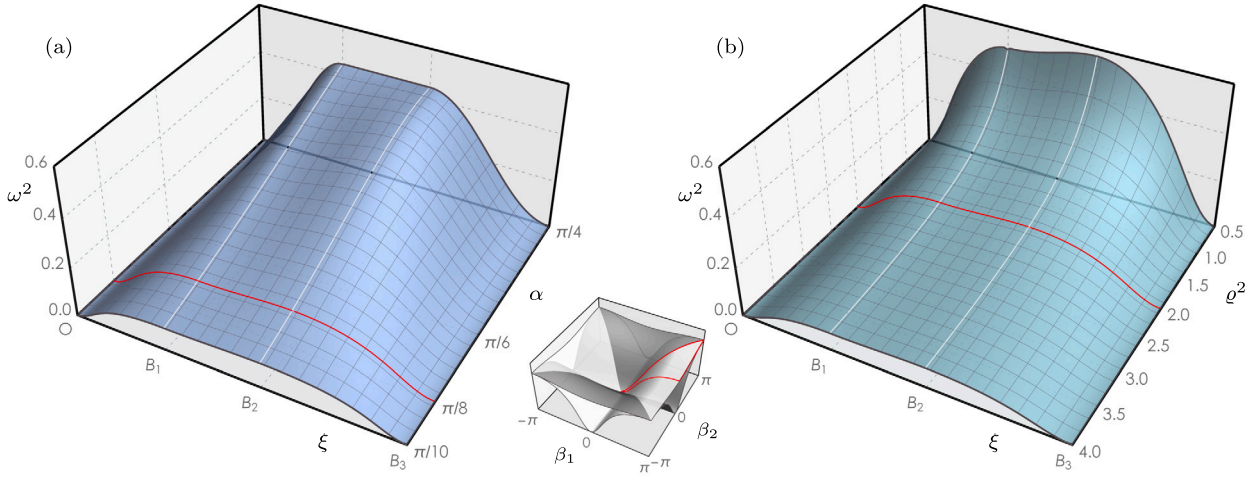

Fig. 3. Linear dispersion curves of the mechanical metamaterial: (a) frequency $\omega_a^2(\xi)$ for varying amplification angles α and fixed mass ratio $\varrho^2 = 2$, (b) frequency $\omega_a^2(\xi)$ for varying mass ratio ϱ^2 and fixed amplification angle $\alpha = \pi/8$.

From the physical viewpoint, the first-order solution provides the dispersion relations expressing the linear (amplitude-independent) frequencies $\omega_a^2(\boldsymbol{\beta})$ and $\omega_c^2(\boldsymbol{\beta})$ of the mono-harmonic waves freely propagating with wavevector $\boldsymbol{\beta}$ through the two-dimensional metamaterial characterized by the mechanical parameters (α, ϱ^2). The *linear frequency spectrum* of the metamaterial is fully characterized by the acoustic dispersion surfaces $\mathcal{S}_a$ and $\mathcal{S}_c$ mapping the positive-valued functions $\omega_a(\boldsymbol{\beta})$ and $\omega_c(\boldsymbol{\beta})$ over the nondimensional first Brillouin zone $\mathcal{B} = \{\boldsymbol{\beta} \in [-\pi, \pi] \times [-\pi, \pi]\}$. As a major qualitative remark, the dispersion spectrum possesses a 4-order rotational symmetry in the frequency-wavevector space (Fig. 2a). From the quantitative viewpoint, the acoustic dispersion surfaces $\mathcal{S}_a$ (purple) and $\mathcal{S}_c$ (pink) cover the same low frequency range, or *frequency pass-band*, bounded by the maximum frequency $\omega_m^2 = 8\sin^2(2\alpha)/[1 + 12\varrho^2 - (1 - 4\varrho^2)\cos(4\alpha)]$. As complementary remark, the parameter-independent locus $\mathcal{R}_1 := \{\boldsymbol{\beta} : \beta_1 = \pm\beta_2\}$ can be proved to satisfy the internal 1:1 resonance condition $\omega_a = \omega_c$ in the dispersion spectrum (dashed black lines). Finally, the vector field of the nondimensional group velocities $\mathbf{c}_a(\boldsymbol{\beta}) = \partial\omega_a(\boldsymbol{\beta})/\partial\boldsymbol{\beta}$ and $\mathbf{c}_c(\boldsymbol{\beta}) = \partial\omega_c(\boldsymbol{\beta})/\partial\boldsymbol{\beta}$ is largely and nonlinearly dependent on the wavevector $\boldsymbol{\beta}$ (Fig. 2b), demonstrating the dispersive nature of the metamaterial.

Parametric analyses of the metamaterial spectrum can be carried out by discussing the dispersion function $\omega_a^2(\xi)$, or equivalently the companion function $\omega_c^2(\xi)$, under variation of the nondimensional *reduced wavenumber* $\xi \in [0, (2 + \sqrt{2})\pi]$, expressing the curvilinear abscissa spanning the closed boundary of the triangular region $\mathcal{B}_0 \subset \mathcal{B}$, defined by the vertices O (at wavevector $\boldsymbol{\beta} = (0, 0)$ or reduced wavevector $\xi = 0$), B_1 (at $\boldsymbol{\beta} = (\pi, 0)$ or $\xi = \pi$), B_2 (at $\boldsymbol{\beta} = (\pi, \pi)$ or $\xi = 2\pi$), $B_3 = O$ (at $\boldsymbol{\beta} = (0, 0)$ or $\xi = (2 + \sqrt{2})\pi$). The parametric results show that increasing amplification angles α amplify the *pass-bandwidth* (Fig. 3a). Growing amplification angles α also correspond to larger group velocity of wave propagation, especially in the range of mid wavelengths. Differently, increments of the

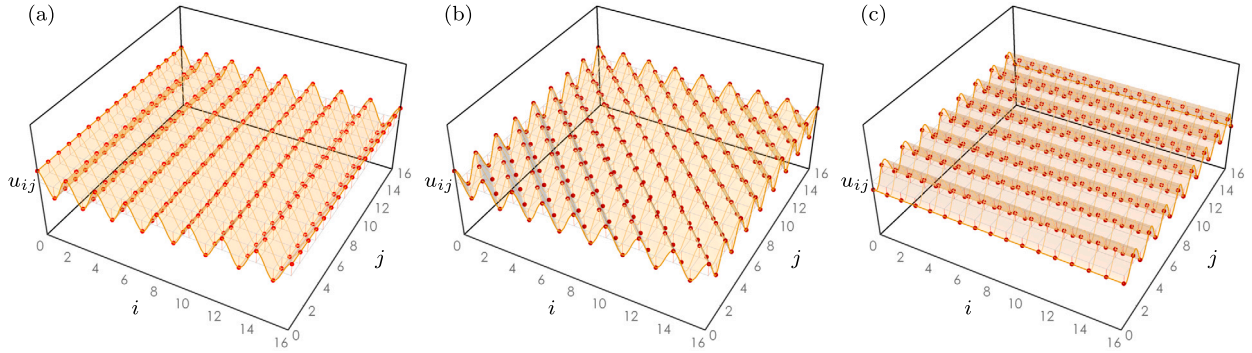

Fig. 4. Linear u-polarized waves propagating in the mechanical metamaterial (for mass ratio $\varrho^2 = 2$ and amplification angle $\alpha = \pi/8$): (a) wavevector $\boldsymbol{\beta} = (\pi, 0)$, (b) wavevector $\boldsymbol{\beta} = (\pi, \pi)$, (c) wavevector $\boldsymbol{\beta} = (0, \pi)$.

mass ratio ϱ^2 reduce the pass-bandwidths (Fig. 3b), and also determine lower group velocities, especially in the range of long wavelengths. From the functional viewpoint, this interesting scenario discloses that large mass ratios (realized, for instance, by light primary atoms connected with heavy secondary atoms), associated to small amplification angles, tend to minimize the pass-bandwidth. This finding paves the way for employing inertia amplification mechanisms in parametrically designing and microstructurally optimizing two-dimensional mechanical metafilters [20].

3.2. Nonlinear dynamics

The perfect polarization of the two linear waveforms $\boldsymbol{\phi}_a$ and $\boldsymbol{\phi}_c$ indicates that each mono-harmonic freely-propagating linear wave is contributed by only one *or* the other degrees-of-freedom of the principal atoms, according to the formulas $\mathbf{a}_1 \pm \imath\mathbf{b}_1 = (a_1 \pm \imath b_1)\,\boldsymbol{\phi}_a$, or $\mathbf{a}_1 \pm \imath\mathbf{b}_1 = (c_1 \pm \imath d_1)\,\boldsymbol{\phi}_c$. Specifically, linear mono-harmonic waves propagating with frequency ω_a or ω_c are characterized either by perfect *u-polarization* ($c_1 = d_1 = 0$) or *v-polarization* ($a_1 = b_1 = 0$), respectively. Perfectly *u-polarized* linear waves freely propagating with harmonic frequency $\omega_a(\boldsymbol{\beta})$ at the two limits of short wavelengths (longitudinal wave for wavevectors $\boldsymbol{\beta} = (\pi, 0)$ and mixed wave for $\boldsymbol{\beta} = (\pi, \pi)$) are illustrated in Figs. 4a, b.

From the physical viewpoint it is interesting to note that perfectly polarized harmonic waves can propagate as pure kinematic modes (unconstrained motions associated to kinematic indeterminacy, known also as *floppy* modes in crystalline glass materials [37], or *rigid unit phonon modes* in network materials [38]). Indeed, perfectly u-polarized waves can freely propagate with vanishing frequency $\omega_a(\boldsymbol{\beta}) = 0$ for all wavevectors $\boldsymbol{\beta}$ of the locus $\mathcal{B}_2 := \{\boldsymbol{\beta} : \beta_1 = 0\}$. Symmetrically, perfectly v-polarized harmonic waves can freely propagate with vanishing frequency $\omega_c(\boldsymbol{\beta}) = 0$ for all wavevectors $\boldsymbol{\beta}$ of the locus $\mathcal{B}_1 := \{\boldsymbol{\beta} : \beta_2 = 0\}$. Such a zero-frequency kinematic propagation of perfectly polarized transverse waves is a remarkable dynamic phenomenon – peculiar of the linear field – caused by the *essentially nonlinear* nature of the elastic stiffnesses acting in the polarization-orthogonal direction. The perfectly u-polarized linear wave propagating kinematically at the limit of short wavelengths (transversal wave for wavevector $\boldsymbol{\beta} = (0, \pi)$) is illustrated in Figs. 4c.

The physical consequence of perfect polarization is that, if perfectly polarized initial conditions are applied, the linear response develops mono-harmonically in time, without any contribution of the degree-of-freedom initially null (polarized response). In contrast, if generic (non-polarized) initial conditions are applied, the linear response develops as a bi-harmonic superposition of freely propagating waves, contributed by both degrees-of-freedom (non-polarized response). Starting from this reference scenario and considering the impossibility of superimposing effects beyond the linear range, the nonlinear response is analyzed by considering general linear solutions (amplitudes a_1, b_1, c_1, d_1 not null a priori), valid for one or the other polarization. The particular polarization is selected (by nullifying c_1, d_1 *or* a_1, b_1) and discussed a posteriori. The primary objective of the discussion is to understand whether non-polarized superharmonic terms in the nonlinear response (*superharmonic depolarization*) can be generated by perfectly polarized harmonic solutions of the linear response. A complementary objective is to verify whether the essential nonlinear stiffness annihilates the possibility of zero-frequency kinematic propagation of perfectly polarized waves, by determining amplitude-dependent increments of the linearly vanishing frequencies.

As final preliminary consideration, it is important to remark that quadratic and cubic nonlinearities may activate extra internal resonances. Indeed, four parameter-dependent loci, defined $\mathcal{R}_2^a := \{\boldsymbol{\beta} : \omega_a(\boldsymbol{\beta}) = 2\omega_c(\boldsymbol{\beta})\}$, $\mathcal{R}_2^c := \{\boldsymbol{\beta} : 2\omega_a(\boldsymbol{\beta}) = \omega_c(\boldsymbol{\beta})\}$ and $\mathcal{R}_3^a := \{\boldsymbol{\beta} : \omega_a(\boldsymbol{\beta}) = 3\omega_c(\boldsymbol{\beta})\}$, $\mathcal{R}_3^c := \{\boldsymbol{\beta} : 3\omega_a(\boldsymbol{\beta}) = \omega_c(\boldsymbol{\beta})\}$ can be proved to co-exist and realize integer ratios (superharmonic resonances 1:2 and 1:3, or subharmonic resonances 2:1 and 3:1) between the linear frequencies. The resonant loci $\mathcal{R}_2^a$, $\mathcal{R}_2^c$ (blue surfaces) and $\mathcal{R}_3^a$, $\mathcal{R}_3^c$ (red surfaces), that naturally differ from the locus $\mathcal{R}_1$ (wireframe surfaces), are illustrated in Fig. 5 over the entire Brillouin zone $\mathcal{B}$ for varying mechanical parameters. Specifically, all the loci can be recognized to depend significantly on the amplification angle α. Other parametric analyses – here not reported for the sake of synthesis – show instead that all the resonant loci are almost independent of the mass ratio ϱ^2. Particular cases of internal (superharmonic or subharmonic) resonances may activate interesting phenomena of wave-wave interactions, like energy tunneling and trapping [35,39,40], but also require a special mathematical treatment in the context of the perturbation strategy, which is beyond the objectives of the present work.

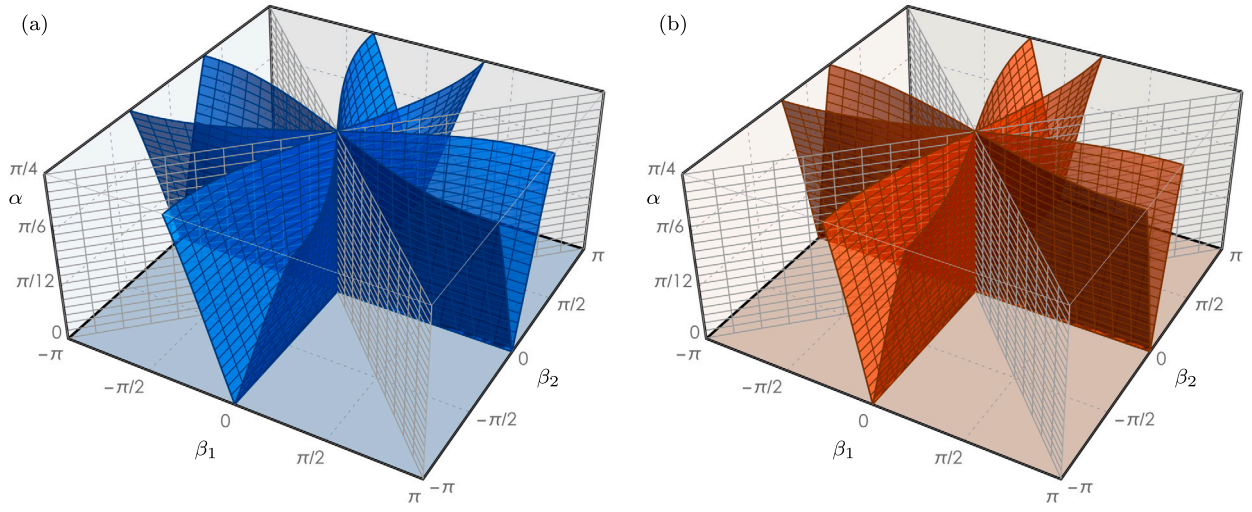

Fig. 5. Loci of internal resonance between the linear frequencies of the mechanical metamaterial (for varying amplification angles α and fixed mass ratio $\varrho^2 = 2$): (a) Loci $\mathcal{R}_1$ (wireframe), $\mathcal{R}_2^a$ and $\mathcal{R}_2^c$ (blue), (b) Loci $\mathcal{R}_1$ (wireframe), $\mathcal{R}_3^a$ and $\mathcal{R}_3^c$ (red).

The second order of the perturbation equations state a pair of identical linear equations expressed in the form $\mathbf{H}(2\omega,\boldsymbol{\beta})\,\mathbf{a}_2 = \mathbf{f}_2(\omega,\boldsymbol{\beta},\mathbf{a}_1,\mathbf{b}_1)$ and $\mathbf{H}(2\omega,\boldsymbol{\beta})\,\mathbf{b}_2 = \mathbf{g}_2(\omega,\boldsymbol{\beta},\mathbf{a}_1,\mathbf{b}_1)$ in the unknown second superharmonic amplitudes $\mathbf{a}_2$ and $\mathbf{b}_2$. Mathematically, the coefficient matrix $\mathbf{H}(2\omega,\boldsymbol{\beta})$ cannot be singular in the general case, provided that the linear frequency ω satisfies one of the dispersion relations (12)-(13) and excluding superharmonic and subharmonic resonance conditions. Consequently, the solutions achievable by matrix inversion as $\mathbf{a}_2 = \mathbf{H}(2\omega,\boldsymbol{\beta})^{-1}\mathbf{f}_2(\omega,\boldsymbol{\beta},\mathbf{a}_1,\mathbf{b}_1)$ and $\mathbf{b}_2 = \mathbf{H}(2\omega,\boldsymbol{\beta})^{-1}\mathbf{g}_2(\omega,\boldsymbol{\beta},\mathbf{a}_1,\mathbf{b}_1)$ are univocally defined, but are parametrically dependent on the amplitudes $\mathbf{a}_1$ and $\mathbf{b}_1$ that remain undetermined. Therefore, considering a priori the generic (non polarized) linear wave with initial amplitude $\mathbf{a}_1 \pm \imath\mathbf{b}_1 = (a_1 \pm \imath b_1)\,\boldsymbol{\phi}_a + (c_1 \pm \imath d_1)\,\boldsymbol{\phi}_c$ at time $\tau = 0$, the solutions for the second superharmonic amplitudes read, in component form

$$
\begin{aligned}
a_2 &= 2\mathcal{A}_{21}a_1b_1 + \mathcal{A}_{22}(a_1d_1 + b_1c_1) + 2\mathcal{A}_{23}c_1d_1 \\
b_2 &= \mathcal{A}_{21}(b_1^2 - a_1^2) + \mathcal{A}_{22}(b_1d_1 + a_1c_1) + \mathcal{A}_{23}(d_1^2 - c_1^2) \\
c_2 &= 2\mathcal{C}_{21}c_1d_1 + \mathcal{C}_{22}(a_1d_1 + b_1c_1) + 2\mathcal{C}_{23}a_1b_1 \\
d_2 &= \mathcal{C}_{21}(d_1^2 - c_1^2) + \mathcal{C}_{22}(b_1d_1 + a_1c_1) + \mathcal{C}_{23}(b_1^2 - a_1^2)
\end{aligned}
\tag{14}
$$

where the superharmonic amplitudes a_2, b_2 and c_2, b_2 are quadratic functions of all the harmonic amplitudes a_1, b_1, c_1, d_1. Therefore, the second superharmonic amplitudes will be referred to also as *quadratic* amplitudes in the following. The coefficients multiplying quadratic terms depend explicitly and implicitly (through the linear frequency) on the mechanical parameters and wavevector, according to the analytical expressions

$$
\begin{aligned}
\mathcal{A}_{21}(\omega) &= 48\varrho^2\omega^2\cos^2(\alpha)\cot^2(\alpha)\sin\beta_1(1-\cos\beta_1)\,\Delta_1^{-1} \\
\mathcal{A}_{22}(\omega) &= 8\sin\beta_2(1-\cos\beta_2)\left[2\varrho^2\omega^2\left(\cos^2(\alpha)-5\sin^2(\alpha)\right)-\sin^2(2\alpha)\right]\Delta_1^{-1} \\
\mathcal{A}_{23}(\omega) &= 4\sin\beta_1(1-\cos\beta_1)\left[4\varrho^2\omega^2\left(2\cos^2(\alpha)-\sin^2(\alpha)\right)-\sin^2(2\alpha)\right]\Delta_1^{-1} \\
\mathcal{C}_{21}(\omega) &= 48\varrho^2\omega^2\cos^2(\alpha)\cot^2(\alpha)\sin\beta_2(1-\cos\beta_2)\,\Delta_2^{-1} \\
\mathcal{C}_{22}(\omega) &= 8\sin\beta_1(1-\cos\beta_1)\left[2\varrho^2\omega^2\left(\cos^2(\alpha)-5\sin^2(\alpha)\right)-\sin^2(2\alpha)\right]\Delta_2^{-1} \\
\mathcal{C}_{23}(\omega) &= 4\sin\beta_2(1-\cos\beta_2)\left[4\varrho^2\omega^2\left(2\cos^2(\alpha)-\sin^2(\alpha)\right)-\sin^2(2\alpha)\right]\Delta_2^{-1} \\
\Delta_1(\omega) &= \left[4\sin^2(2\alpha)\left(1-2\omega^2-\cos\beta_1\right)-32\varrho^2\omega^2\left(1-\cos(2\alpha)\left(\cos^2(\alpha)\cos\beta_1-\sin^2(\alpha)\cos\beta_2\right)\right)\right] \\
\Delta_2(\omega) &= \left[4\sin^2(2\alpha)\left(1-2\omega^2-\cos\beta_2\right)-32\varrho^2\omega^2\left(1-\cos(2\alpha)\left(\cos^2(\alpha)\cos\beta_2-\sin^2(\alpha)\cos\beta_1\right)\right)\right]
\end{aligned}
\tag{15}
$$

where relations $\Delta_1 = F_a(2\omega,\boldsymbol{\beta})$ and $\Delta_2 = F_c(2\omega,\boldsymbol{\beta})$ hold for the denominators. Consequently, perturbation solutions (14) become asymptotically inconsistent if internal superharmonic 1:2 and subharmonic 2:1 resonance (or quasi-resonance) conditions occur (*small denominators*). Therefore, loci $\mathcal{R}_2^a$ and $\mathcal{R}_2^c$ (and their closest neighborhood) have to be excluded from the validity region of the perturbation solutions (14).

The particular cases of u-polarized linear wave propagating with complex conjugate amplitudes $\mathbf{a}_1 \pm \imath\mathbf{b}_1 = (a_1 \pm \imath b_1)\,\boldsymbol{\phi}_a$ and frequency $\omega_a(\boldsymbol{\beta})$ can be analyzed first. The perfect u-polarization significantly simplifies the higher-order solutions, due to null contribution of the polarization-orthogonal linear amplitudes ($c_1 = d_1 = 0$). Consequently, second-order solutions (14) assume the

Table 1
Superharmonic amplitudes of the linearly polarized solutions.

Polarization	Second order	Third order
u-polarization	$a_2 = 2\mathcal{A}^a_{21} a_1 b_1$	$a_3 = \mathcal{A}^a_{31} a_1(3b_1^2 - a_1^2) + \mathcal{A}^a_{33}(a_2 b_1 + a_1 b_2) + \mathcal{A}^a_{34}(a_1 d_2 + c_2 b_1) = -\mathcal{A}^a_{37} a_1^3 + \mathcal{A}^a_{38} a_1 b_1^2$
$\mathbf{a}_1 \pm \imath \mathbf{b}_1 = (a_1 \pm \imath b_1)\,\boldsymbol{\phi}_a$	$b_2 = \mathcal{A}^a_{21}(b_1^2 - a_1^2)$	$b_3 = \mathcal{A}^a_{31} b_1(b_1^2 - 3a_1^2) + \mathcal{A}^a_{33}(b_1 b_2 - a_1 a_2) + \mathcal{A}^a_{34}(b_1 d_2 - a_1 c_2) = \mathcal{A}^a_{37} b_1^3 - \mathcal{A}^a_{38} a_1^2 b_1$
	$c_2 = 2C^a_{23} a_1 b_1$	$c_3 = C^a_{35}(a_1 d_2 + b_1 c_2) + C^a_{36}(a_1 b_2 + a_2 b_1) = -C^a_{37} a_1^3 + C^a_{38} a_1 b_1^2$
	$d_2 = C^a_{23}(b_1^2 - a_1^2)$	$d_3 = C^a_{35}(b_1 d_2 - a_1 c_2) + C^a_{36}(b_1 b_2 - a_1 a_2) = C^a_{37} b_1^3 - C^a_{38} a_1^2 b_1$
v-polarization	$a_2 = 2\mathcal{A}^c_{23} c_1 d_1$	$a_3 = \mathcal{A}^c_{35}(c_1 b_2 + a_2 d_1) + \mathcal{A}^c_{36}(c_2 d_1 + c_1 d_2) = -\mathcal{A}^c_{37} c_1^3 + \mathcal{A}^c_{38} c_1 d_1^2$
$\mathbf{a}_1 \pm \imath \mathbf{b}_1 = (c_1 \pm \imath d_1)\,\boldsymbol{\phi}_c$	$b_2 = \mathcal{A}^c_{23}(d_1^2 - c_1^2)$	$b_3 = \mathcal{A}^c_{35}(b_2 d_1 - a_2 c_1) + \mathcal{A}^c_{36}(d_1 d_2 - c_1 c_2) = \mathcal{A}^c_{37} d_1^3 - \mathcal{A}^c_{38} c_1^2 d_1$
	$c_2 = 2C^c_{21} c_1 d_1$	$c_3 = C^c_{31} c_1(3d_1^2 - c_1^2) + C^c_{33}(c_1 d_2 + c_2 d_1) + C^c_{34}(a_2 d_1 + b_2 c_1) = -C^c_{37} c_1^3 + C^c_{38} c_1 d_1^2$
	$d_2 = C^c_{21}(d_1^2 - c_1^2)$	$d_3 = C^c_{31} d_1(d_1^2 - 3c_1^2) + C^c_{33}(d_1 d_2 - c_1 c_2) + C^c_{34}(b_2 d_1 - a_2 c_1) = C^c_{37} d_1^3 - C^c_{38} c_1^2 d_1$

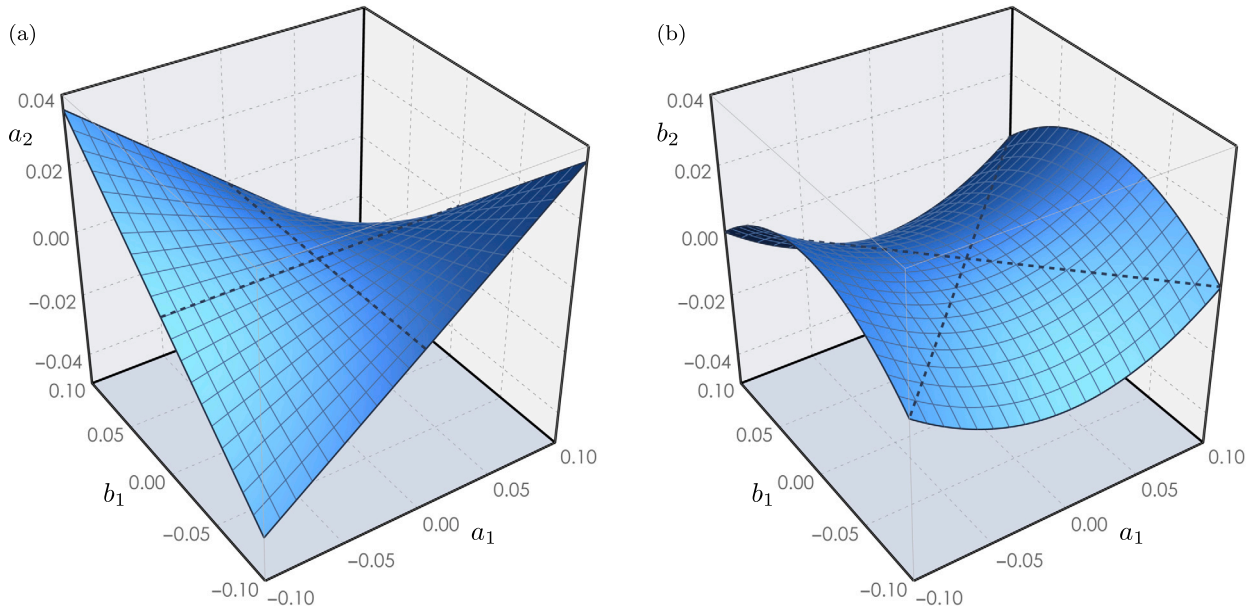

Fig. 6. Superharmonic amplitudes a_2 and b_2 for the mechanical metamaterial (for mass ratio $\varrho^2 = 2$ and amplification angle $\alpha = \pi/5$ at wavevector $\boldsymbol{\beta} = (5/6\pi, 1/2\pi)$, corresponding to non-resonant linear frequencies ($\omega_a/\omega_c = 1.216$ or $\omega_c/\omega_a = 0.822$): (a) surface $\mathcal{Q}_a$ (blue surface) and locus $\mathcal{N}_a$ (dashed lines), (b) surface $\mathcal{Q}_b$ (blue surface) and locus $\mathcal{N}_b$ (dashed lines).

reduced form reported in Table 1 (upper rows), where coefficients $\mathcal{A}^a_{hk} = \mathcal{A}_{hk}(\omega_a)$ and $C^a_{hk} = C_{hk}(\omega_a)$. Predictably, the solutions describe a superharmonic wave arising and propagating with double frequency $2\omega_a(\boldsymbol{\beta})$, or half period. Remarkably, the superharmonic wave propagates with polarization-collinear amplitudes $a_2 = 2\mathcal{A}^a_{21} a_1 b_1$ and $b_2 = \mathcal{A}^a_{21}(b_1^2 - a_1^2)$, as well as polarization-orthogonal amplitudes $c_2 = 2C^a_{23} a_1 b_1$ and $d_2 = C^a_{23}(b_1^2 - a_1^2)$. The activation of polarization-orthogonal amplitudes discloses that polarized waves in the linear field systematically generate non polarized waves in the nonlinear field. The depolarization phenomenon does not require the occurrence of internal resonance, nor the onset of any period-halving bifurcation. In synthesis, depolarization occurs at the second order as natural consequence of pure quadratic coupling in the nonlinear equations.

The quadratic functions $a_2 = 2\mathcal{A}^a_{21} a_1 b_1$ and $b_2 = \mathcal{A}^a_{21}(b_1^2 - a_1^2)$ describe a pair of smooth surfaces, denoted $\mathcal{Q}_a$ and $\mathcal{Q}_b$ respectively, over the (a_1, b_1)-domain. Fig. 6 illustrates surfaces $\mathcal{Q}_a$ and $\mathcal{Q}_b$ for a certain wavevector and a significant parameter set. From the geometric viewpoint, $\mathcal{Q}_a$ and $\mathcal{Q}_b$ are saddle surfaces (precisely *hyperbolic paraboloids*), characterized by negative Gaussian curvature at every point. In the origin, surfaces $\mathcal{Q}_a$ and $\mathcal{Q}_b$ are tangent to the null planes (with equations $a_2 = 0$ and $b_2 = 0$, respectively), where linear wave motions live. Furthermore, two loci $\mathcal{N}_a = \{(a_1, b_1) \colon a_1 = 0 \vee b_1 = 0\}$ and $\mathcal{N}_b = \{(a_1, b_1) \colon a_1 \pm b_1\}$ of linear harmonic amplitudes can be recognized to determine systematically null superharmonic amplitudes ($a_2 = 0$ and $b_2 = 0$, respectively), regardless of the mechanical parameter values.

The other quadratic functions $c_2 = 2C^a_{23} a_1 b_1$ and $d_2 = C^a_{23}(b_1^2 - a_1^2)$ describe a pair of companion surfaces, denoted $\mathcal{Q}_c$ and $\mathcal{Q}_d$ respectively. By mathematical construction, surfaces $\mathcal{Q}_c$ and $\mathcal{Q}_d$ are identical to surfaces $\mathcal{Q}_a$ and $\mathcal{Q}_b$, respectively, except for the scaling factor $r^a_2 = c_2/a_2 = d_2/b_2 = C^a_{23}/\mathcal{A}^a_{21}$, which plays the role of *second-order depolarization factor*. From the quantitative viewpoint, the depolarization factor r^a_2 generally (but depending on the wavevector $\boldsymbol{\beta}$) attains small values over almost the entire range of mechanical parameters. Consequently, the nonlinear depolarization generated by the superharmonic amplitudes tends to be a slight – although appreciable – dynamic phenomenon. Fig. 7a illustrates the variability of the depolarization factor r^a_2 for wavevector $\boldsymbol{\beta} = (5/6\pi, 1/2\pi)$. Interestingly, the nonlinear depolarization mainly depends on the amplification angle α, whereas it is less or minimally dependent

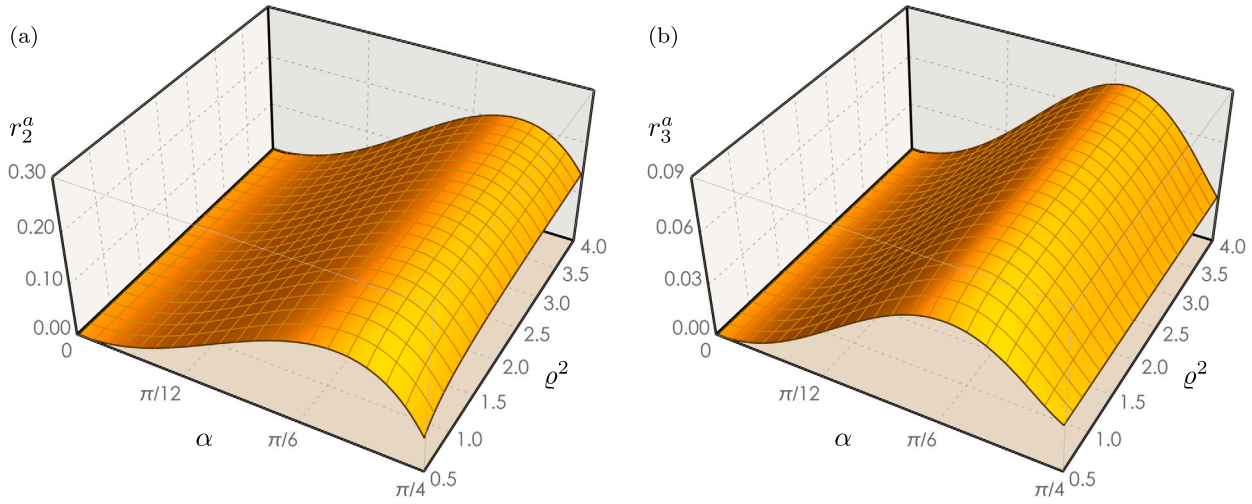

Fig. 7. Depolarization factors over the range of mechanical parameters for multi-harmonic waves propagating with wavevector $\boldsymbol{\beta} = (5/6\pi, 1/2\pi)$ the wave: (a) second-order depolarization factor r_2^a, (b) third-order depolarization factor r_3^a.

on the mass ratio ϱ^2. As direct consequence, the nonlinear depolarization effect could be exalted by maximizing the known function $r_2^a(\alpha, \varrho^2)$ with respect to the amplification, using the mass ratios as parameter. The depolarization-maximizing loci in the mechanical parameter space vary with the wavevector, but are determinable analytically (apart the cumbersome algebra) or numerically (e.g. $\alpha \simeq 0.620$, close to $\alpha = \pi/5$ in Fig. 7a).

Similar qualitative and quantitative considerations can be pointed out for the complementary case concerning υ-polarized linear waves. The perfect υ-polarization simplifies the higher-order solutions, due to null contribution of the polarization-orthogonal linear amplitudes ($a_1 = b_1 = 0$). Consequently, solutions (14) assume the reduced form reported in Table 1 (lower rows), where $\mathcal{A}_{hk}^c = \mathcal{A}_{hk}(\omega_c)$ and $C_{hk}^c = C_{hk}(\omega_c)$. As a minor difference, the second-order depolarization factor reads $r_2^c = a_2/c_2 = b_2/d_2 = \mathcal{A}_{23}^c/C_{21}^c$.

The third order of the perturbation equations state a pair of identical linear equations expressed in the form $\mathbf{H}(3\omega, \boldsymbol{\beta})\,\mathbf{a}_3 = \mathbf{f}_3(\omega, \boldsymbol{\beta}, \mathbf{a}_1, \mathbf{b}_1, \mathbf{a}_2, \mathbf{b}_2)$ and $\mathbf{H}(3\omega, \boldsymbol{\beta})\,\mathbf{b}_3 = \mathbf{g}_3(\omega, \boldsymbol{\beta}, \mathbf{a}_1, \mathbf{b}_1, \mathbf{a}_2, \mathbf{b}_2)$ in the unknown second superharmonic amplitudes $\mathbf{a}_3$ and $\mathbf{b}_3$. Mathematically, the coefficient matrix $\mathbf{H}(3\omega, \boldsymbol{\beta})$ cannot be singular in the general case, provided that the linear frequency ω satisfies one of the dispersion relations (12)-(13) and excluding superharmonic and subharmonic resonance conditions. Consequently, the solutions achievable by matrix inversion as $\mathbf{a}_3 = \mathbf{H}(3\omega, \boldsymbol{\beta})^{-1}\mathbf{f}_3(\omega, \boldsymbol{\beta}, \mathbf{a}_1, \mathbf{b}_1, \mathbf{a}_2, \mathbf{b}_2)$ and $\mathbf{b}_3 = \mathbf{H}(3\omega, \boldsymbol{\beta})^{-1}\mathbf{g}_3(\omega, \boldsymbol{\beta}, \mathbf{a}_1, \mathbf{b}_1, \mathbf{a}_2, \mathbf{b}_2)$ are univocally defined. By recalling that $\mathbf{a}_2 = \mathbf{H}(2\omega, \boldsymbol{\beta})^{-1}\mathbf{f}_2(\omega, \boldsymbol{\beta}, \mathbf{a}_1, \mathbf{b}_1)$ and $\mathbf{b}_2 = \mathbf{H}(2\omega, \boldsymbol{\beta})^{-1}\mathbf{g}_2(\omega, \boldsymbol{\beta}, \mathbf{a}_1, \mathbf{b}_1)$, according to the second order solution, the third order solutions $\mathbf{a}_3$ and $\mathbf{b}_3$ end up to parametrically depend on the amplitudes $\mathbf{a}_1$ and $\mathbf{b}_1$ that remain undetermined. Therefore, considering a priori a generic (non polarized) linear wave with initial amplitude $\mathbf{a}_1 \pm \imath\mathbf{b}_1 = (a_1 \pm \imath b_1)\,\boldsymbol{\phi}_a + (c_1 \pm \imath d_1)\,\boldsymbol{\phi}_c$ at time $\tau = 0$, the solutions for the second superharmonic amplitudes read, in component form

$$
\begin{aligned}
a_3 =& \mathcal{A}_{31}a_1(3b_1^2 - a_1^2) + \mathcal{A}_{32}\big[a_1(d_1^2 - c_1^2) + 2b_1c_1d_1\big] + \\
&+ \mathcal{A}_{33}(a_2b_1 + a_1b_2) + \mathcal{A}_{34}(a_1d_2 + c_2b_1) + \mathcal{A}_{35}(c_1b_2 + a_2d_1) + \mathcal{A}_{36}(c_2d_1 + c_1d_2) \\
b_3 =& \mathcal{A}_{31}b_1(b_1^2 - 3a_1^2) + \mathcal{A}_{32}\big[b_1(d_1^2 - c_1^2) - 2a_1c_1d_1\big] + \\
&+ \mathcal{A}_{33}(b_1b_2 - a_1a_2) + \mathcal{A}_{34}(b_1d_2 - a_1c_2) + \mathcal{A}_{35}(b_2d_1 - a_2c_1) + \mathcal{A}_{36}(d_1d_2 - c_1c_2) \\
c_3 =& C_{31}c_1(3d_1^2 - c_1^2) + C_{32}\big[c_1(b_1^2 - a_1^2) + 2a_1b_1d_1\big] + \\
&+ C_{33}(c_1d_2 + c_2d_1) + C_{34}(a_2d_1 + b_2c_1) + C_{35}(a_1d_2 + b_1c_2) + C_{36}(a_1b_2 + a_2b_1) \\
d_3 =& C_{31}d_1(d_1^2 - 3c_1^2) + C_{32}\big[d_1(b_1^2 - a_1^2) - 2a_1b_1c_1\big] + \\
&+ C_{33}(d_1d_2 - c_1c_2) + C_{34}(b_2d_1 - a_2c_1) + C_{35}(b_1d_2 - a_1c_2) + C_{36}(b_1b_2 - a_1a_2)
\end{aligned}
\tag{16}
$$

where the superharmonic amplitudes a_3, b_3 and c_3, b_3 are cubic functions of all the harmonic amplitudes a_1, b_1, c_1, d_1 and superharmonic amplitudes a_2, b_2, c_2, d_2. Therefore, the third superharmonic amplitudes will be referred to also as *cubic* amplitudes in the following. The coefficients multiplying cubic terms depend explicitly and implicitly (through the linear frequency) on the mechanical parameters and wavevector, according to the analytical expressions

$$
\begin{aligned}
\mathcal{A}_{31} = \big[&4\varrho^2\omega^2\csc^2(\alpha)\big(6 + 4\csc^4(\alpha) - 7\csc^2(\alpha) - 2\sec^2(\alpha)\big) + \\
&+ 2(1 + 2\cos\beta_2)\big(3 - 4\cos\beta_2 + \cos(2\beta_2)\big) + \\
&- 2\varrho^2\omega^2\cot^2(\alpha)\csc^4(\alpha)\big(5 + 3\cos(2\alpha)\big)\big(3\cos\beta_1 - 3\cos(2\beta_1) + \cos(3\beta_1)\big) + \\
&+ 2\varrho^2\omega^2\csc^2(\alpha)\sec^2(\alpha)\big(1 - 3\cos(2\alpha)\big)\big(3\cos\beta_2 - 3\cos(2\beta_2) + \cos(3\beta_2)\big)\big]\Delta_3^{-1}
\end{aligned}
\tag{17}
$$

$$
\begin{aligned}
\mathcal{A}_{32} &= \big[8-4\varrho^2\omega^2\left(8\csc^2(\alpha)-5\csc^4(\alpha)-10\sec^2(\alpha)\right)+\\
&\quad+4\big(3\cos\beta_1-3\cos(2\beta_1)+\cos(3\beta_1)\big)-4\big(3\cos\beta_2-3\cos(2\beta_2)+\cos(3\beta_2)\big)+\\
&\quad-\varrho^2\omega^2\csc^4(\alpha)\sec^2(\alpha)\big(3\cos\beta_1-3\cos(2\beta_1)+\cos(3\beta_1)\big)\big(\cos(2\alpha)+4\sin^2(2\alpha)+13\cos^2(2\alpha)\big)+\\
&\quad+\varrho^2\omega^2\csc^4(\alpha)\sec^2(\alpha)\big(3\cos\beta_2-3\cos(2\beta_2)+\cos(3\beta_2)\big)\big(11\cos(2\alpha)-8\sin^2(2\alpha)-17\cos^2(2\alpha)\big)\big]\Delta_3^{-1}\\
\mathcal{A}_{33} &= -56\varrho^2\omega^2\cot^2(\alpha)\csc^2(\alpha)\sin\beta_1(1-\cos\beta_1)\Delta_3^{-1}\\
\mathcal{A}_{34} &= 2\csc^2(\alpha)\sec^2(\alpha)\sin\beta_2(1-\cos\beta_2)\left(4\varrho^2\omega^2\left(5\sin^2(\alpha)-2\cos^2(\alpha)\right)+\sin^2(2\alpha)\right)\Delta_3^{-1}\\
\mathcal{A}_{35} &= 2\csc^2(\alpha)\sec^2(\alpha)\sin\beta_2(1-\cos\beta_2)\left(2\varrho^2\omega^2\left(13\sin^2(\alpha)-\cos^2(\alpha)\right)+\sin^2(2\alpha)\right)\Delta_3^{-1}\\
\mathcal{A}_{36} &= 2\csc^2(\alpha)\sec^2(\alpha)\sin\beta_1(1-\cos\beta_1)\left(2\varrho^2\omega^2\left(5\sin^2(\alpha)-9\cos^2(\alpha)\right)+\sin^2(2\alpha)\right)\Delta_3^{-1}\\
\mathcal{C}_{31} &= \big[4\varrho^2\omega^2\csc^2(\alpha)\left(6+4\csc^4(\alpha)-7\csc^2(\alpha)-2\sec^2(\alpha)\right)+\\
&\quad+2(1+2\cos\beta_1)\big(3-4\cos\beta_1+\cos(2\beta_1)\big)+\\
&\quad-2\varrho^2\omega^2\cot^2(\alpha)\csc^4(\alpha)\big(5+3\cos(2\alpha)\big)\big(3\cos\beta_2-3\cos(2\beta_2)+\cos(3\beta_2)\big)+\\
&\quad+2\varrho^2\omega^2\csc^2(\alpha)\sec^2(\alpha)\big(1-3\cos(2\alpha)\big)\big(3\cos\beta_1-3\cos(2\beta_1)+\cos(3\beta_1)\big)\big]\Delta_4^{-1}\\
\mathcal{C}_{32} &= \big[8-4\varrho^2\omega^2\left(8\csc^2(\alpha)-5\csc^4(\alpha)-10\sec^2(\alpha)\right)+\\
&\quad+4\big(3\cos\beta_2-3\cos(2\beta_2)+\cos(3\beta_2)\big)-4\big(3\cos\beta_1-3\cos(2\beta_1)+\cos(3\beta_1)\big)+\\
&\quad-\varrho^2\omega^2\csc^4(\alpha)\sec^2(\alpha)\big(3\cos\beta_2-3\cos(2\beta_2)+\cos(3\beta_2)\big)\big(\cos(2\alpha)+4\sin^2(2\alpha)+13\cos^2(2\alpha)\big)+\\
&\quad+\varrho^2\omega^2\csc^4(\alpha)\sec^2(\alpha)\big(3\cos\beta_1-3\cos(2\beta_1)+\cos(3\beta_1)\big)\big(11\cos(2\alpha)-8\sin^2(2\alpha)-17\cos^2(2\alpha)\big)\big]\Delta_4^{-1}\\
\mathcal{C}_{33} &= -56\varrho^2\omega^2\cot^2(\alpha)\csc^2(\alpha)\sin\beta_2(1-\cos\beta_2)\Delta_4^{-1}\\
\mathcal{C}_{34} &= 2\csc^2(\alpha)\sec^2(\alpha)\sin\beta_1(1-\cos\beta_1)\left(4\varrho^2\omega^2\left(5\sin^2(\alpha)-2\cos^2(\alpha)\right)+\sin^2(2\alpha)\right)\Delta_4^{-1}\\
\mathcal{C}_{35} &= 2\csc^2(\alpha)\sec^2(\alpha)\sin\beta_1(1-\cos\beta_1)\left(2\varrho^2\omega^2\left(13\sin^2(\alpha)-\cos^2(\alpha)\right)+\sin^2(2\alpha)\right)\Delta_4^{-1}\\
\mathcal{C}_{36} &= 2\csc^2(\alpha)\sec^2(\alpha)\sin\beta_2(1-\cos\beta_2)\left(2\varrho^2\omega^2\left(5\sin^2(\alpha)-9\cos^2(\alpha)\right)+\sin^2(2\alpha)\right)\Delta_4^{-1}\\
\Delta_3 &= \big[4(\cos\beta_1-1)+18\omega^2\left(1+4\varrho^2\csc^2(2\alpha)\right)+18\varrho^2\omega^2\cos(2\alpha)\left(\cos\beta_2\sec^2(\alpha)-\cos\beta_1\csc^2(\alpha)\right)\big]\\
\Delta_4 &= \big[4(\cos\beta_2-1)+18\omega^2\left(1+4\varrho^2\csc^2(2\alpha)\right)+18\varrho^2\omega^2\cos(2\alpha)\left(\cos\beta_1\sec^2(\alpha)-\cos\beta_2\csc^2(\alpha)\right)\big]
\end{aligned}
$$

where relations $\Delta_3 = F_a(3\omega,\boldsymbol{\beta})$ and $\Delta_4 = F_c(3\omega,\boldsymbol{\beta})$ hold for the denominators. Consequently, perturbation solutions (16) become asymptotically inconsistent if internal superharmonic 1:3 and subharmonic 3:1 resonance (or quasi-resonance) conditions occur (*small denominators*). Therefore, loci $\mathcal{R}_3^a$ and $\mathcal{R}_3^c$ (and their closest neighborhood) have to be excluded from the validity region of the perturbation solutions (16).

Coherently with the discussion of the second-order solutions, the perfect u-polarization can be analyzed first. Since the polarization-orthogonal amplitudes do not contribute to the u-polarized linear wave ($c_1 = d_1 = 0$), third-order solutions (16) assume the reduced form reported in Table 1 (upper rows), where the auxiliary coefficients $\mathcal{A}_{37}^a = \mathcal{A}_{31}^a + \mathcal{A}_{21}^a\mathcal{A}_{33}^a + \mathcal{A}_{34}^a\mathcal{C}_{23}^a$, $\mathcal{A}_{38}^a = 3\left(\mathcal{A}_{31}^a + \mathcal{A}_{21}^a\mathcal{A}_{33}^a + \mathcal{A}_{34}^a\mathcal{C}_{23}^a\right)$, $\mathcal{C}_{37}^a = \mathcal{A}_{21}^a\mathcal{C}_{36}^a + \mathcal{C}_{23}^a\mathcal{C}_{35}^a$ and $\mathcal{C}_{38}^a = 3\left(\mathcal{A}_{21}^a\mathcal{C}_{36}^a + \mathcal{C}_{23}^a\mathcal{C}_{35}^a\right)$ have been introduced. Predictably, the solutions describe a superharmonic wave arising and propagating with triple frequency $3\omega_a(\boldsymbol{\beta})$. Remarkably, the superharmonic wave propagates with polarization-collinear amplitudes $a_3 = -\mathcal{A}_{37}^a a_1^3 + \mathcal{A}_{38}^a a_1 b_1^2$ and $b_3 = \mathcal{A}_{37}^a b_1^3 - \mathcal{A}_{38}^a a_1 b_1^2$, as well as polarization-orthogonal amplitudes $c_3 = -\mathcal{C}_{37}^a a_1^3 + \mathcal{C}_{38}^a a_1 b_1^2$ and $d_3 = \mathcal{C}_{37}^a b_1^3 - \mathcal{C}_{38}^a a_1 b_1^2$. The activation of polarization-orthogonal amplitudes discloses that polarized waves in the linear fields systematically generate non-polarized waves at the third order, even if the second order depolarization is nullified (for particular parameter combinations zeroing the second-order depolarization factor $r_2^a = \mathcal{C}_{23}^a/\mathcal{A}_{21}^a$). In synthesis, depolarization occurs at the third order as consequence of the cubic nonlinearities, independently of the depolarization effect caused by quadratic nonlinearities at the second order.

The cubic functions $a_3 = -\mathcal{A}_{37}^a a_1^3 + \mathcal{A}_{38}^a a_1 b_1^2$ and $b_3 = \mathcal{A}_{37}^a b_1^3 - \mathcal{A}_{38}^a a_1 b_1^2$ describe a pair of smooth surfaces, denoted $\mathcal{G}_a$ and $\mathcal{G}_b$ respectively, over the (a_1, b_1)-domain. Fig. 8 illustrates surfaces $\mathcal{G}_a$ and $\mathcal{G}_b$ for a certain wavevector and a significant parameter set. From the geometric viewpoint, $\mathcal{G}_a$ and $\mathcal{G}_b$ are saddle surfaces (precisely *monkey saddle* surfaces), characterized by negative Gaussian curvature at every point. In the origin, surfaces $\mathcal{G}_a$ and $\mathcal{G}_b$ have null Gaussian curvature and are tangent to the null planes. Furthermore, two loci $\mathcal{H}_a = \{(a_1,b_1)\colon a_1 = 0 \vee a_1 = \pm\sqrt{3}b_1\}$ and $\mathcal{H}_b = \{(a_1,b_1)\colon b_1 = 0 \vee b_1 = \pm\sqrt{3}a_1\}$ of linear harmonic amplitudes can be recognized to determine systematically null superharmonic amplitudes ($a_3 = 0$ and $b_3 = 0$, respectively), independently of the mechanical parameter values. It is worth noting that, apart some overlapping points (including the origin), the third-order loci $\mathcal{H}_a$ and $\mathcal{H}_b$ do not coincide with second-order loci $\mathcal{N}_a$ and $\mathcal{N}_b$.

The other cubic functions $c_3 = -\mathcal{C}_{37}^a a_1^3 + \mathcal{C}_{38}^a a_1 b_1^2$ and $d_3 = \mathcal{C}_{37}^a b_1^3 - \mathcal{C}_{38}^a a_1 b_1^2$ describe a pair of companion surfaces, denoted $\mathcal{G}_c$ and $\mathcal{G}_d$ respectively. Surfaces $\mathcal{G}_c$ and $\mathcal{G}_d$ are similar to surfaces $\mathcal{G}_a$ and $\mathcal{G}_b$, respectively. Assuming linear amplitudes $b_1 = 0$ for the sake of simplicity, surfaces $\mathcal{G}_c$ and $\mathcal{G}_a$ differ only quantitatively by the scaling factor $r_3^a = c_3/a_3 = \mathcal{C}_{37}^a/\mathcal{A}_{37}^a$, which plays the role of *third-order depolarization factor*. Similarly to the second-order factor, the third-order depolarization factor r_3^a generally (but depending on the wavevector $\boldsymbol{\beta}$) attains small values over almost the entire range of mechanical parameters. Quantitatively, the depolarization factor r_3^a

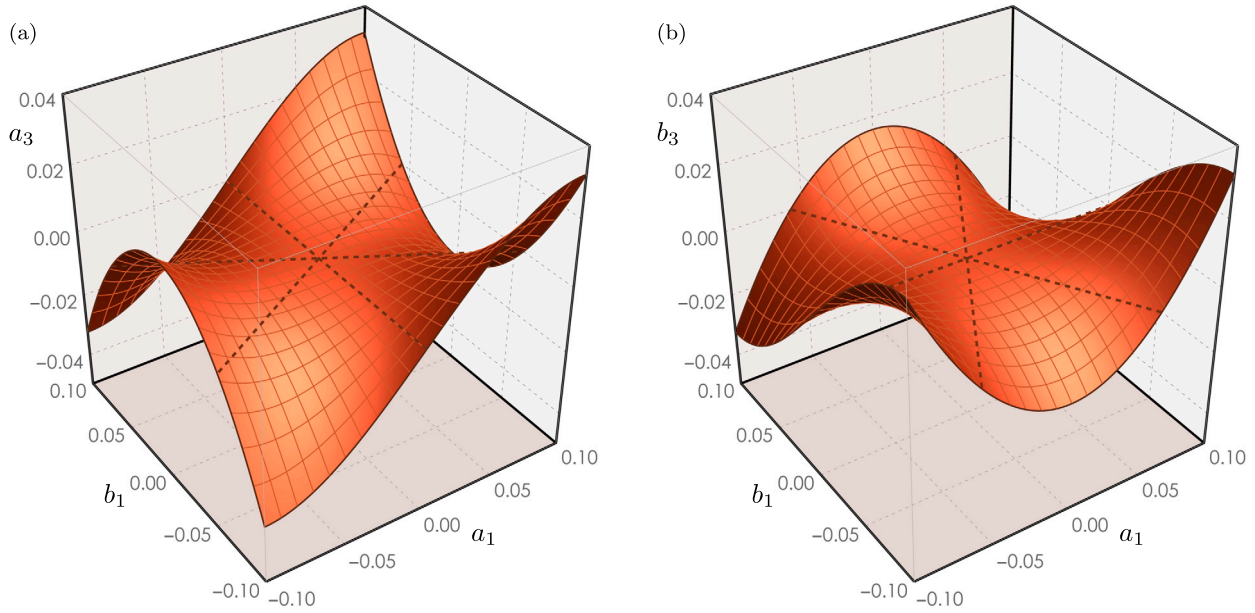

Fig. 8. Superharmonic amplitudes a_3 and b_3 for the mechanical metamaterial (for mass ratio $\varrho^2 = 2$ and amplification angle $\alpha = \pi/5$ at wavevector $\boldsymbol{\beta} = (5/6\pi, 1/2\pi)$, corresponding to non-resonant linear frequencies ($\omega_a/\omega_c = 1.216$ or $\omega_c/\omega_a = 0.822$): (a) surface $\mathcal{G}_a$ (red surface) and locus $\mathcal{H}_a$ (dashed lines), (b) surface $\mathcal{G}_b$ (red surface) and locus $\mathcal{H}_b$ (dashed lines).

depends on the wavevector $\boldsymbol{\beta}$, but generally attains very small values over almost the entire range of mechanical parameters. Similarly to the second-order depolarization factor r_2^a, the third-order depolarization factor r_3^a is mainly dependent on the amplification angle α, whereas it is less dependent on the mass ratio ϱ^2. Fig. 7b illustrates the variability of the depolarization factor r_3^a for wavevector $\boldsymbol{\beta} = (5/6\pi, 1/2\pi)$. Specifically, the amplification angle maximizing the depolarization factor can be determined analytically or numerically, using the mass ratios as parameter. It may be worth noting that the parameter combinations maximizing the depolarization factor r_3^a generally differ (e.g. $\alpha \simeq 0.550$, close to $\alpha = \pi/6$ in Fig. 7b) from those maximizing the second-order depolarization factor r_2^a.

Similar considerations can be pointed out from the complementary case concerning v-polarized linear waves. Symmetrically to the u-polarization, perfect v-polarization simplifies all the higher-order solutions, due to null contribution of polarization-orthogonal linear amplitudes ($a_1 = b_1 = 0$). Consequently, solutions (16) simplify in the form reported in Table 1, where the new auxiliary coefficients $\mathcal{A}_{37}^c = \mathcal{A}_{36}^c C_{21}^c + \mathcal{A}_{23}^c \mathcal{A}_{35}^c$, $\mathcal{A}_{38}^c = 3\left(\mathcal{A}_{36}^c C_{21}^c + \mathcal{A}_{23}^c \mathcal{A}_{35}^c\right)$, $C_{37}^c = C_{31}^c + C_{21}^c C_{33}^c + \mathcal{A}_{23}^c C_{34}^c$ and $C_{38}^c = 3\left(C_{31}^c + C_{21}^c C_{33}^c + \mathcal{A}_{23}^c C_{34}^c\right)$ have been introduced. As a minor difference, the third-order depolarization factor reads $r_3^c = a_3/c_3 = \mathcal{A}_{37}^c / C_{37}^c$ assuming null linear amplitudes $d_1 = 0$ for the sake of simplicity.

3.3. Nonlinear wavefrequencies

Together with the perturbation equations solved to determine the superharmonic amplitudes $\mathbf{a}_3$ and $\mathbf{b}_3$, the third order introduces also two amplitude-dependent corrections perturbing the first-order pair of eigenproblems solved to determine the linear dispersion properties. Specifically, the third order pair of perturbed amplitude-dependent (nonlinear) eigenproblems can be formulated in the standard form

$$\epsilon\left[\mathbf{F}_1(\boldsymbol{\beta}) - \omega^2 \mathbf{G}_1(\boldsymbol{\beta}) + \epsilon^2\left(\mathbf{F}_3(\boldsymbol{\beta}, \mathbf{a}_1, \mathbf{b}_1) - \omega^2 \mathbf{G}_3(\boldsymbol{\beta}, \mathbf{a}_1, \mathbf{b}_1)\right)\right]\mathbf{a}_1 = \mathbf{0} \tag{18}$$

$$\epsilon\left[\mathbf{F}_1(\boldsymbol{\beta}) - \omega^2 \mathbf{G}_1(\boldsymbol{\beta}) + \epsilon^2\left(\mathbf{F}_3(\boldsymbol{\beta}, \mathbf{b}_1, \mathbf{a}_1) - \omega^2 \mathbf{G}_3(\boldsymbol{\beta}, \mathbf{b}_1, \mathbf{a}_1)\right)\right]\mathbf{b}_1 = \mathbf{0} \tag{19}$$

where the unperturbed eigenproblems coincide with the first order eigenproblems (apart for the convenient decomposition $\mathbf{H}(\omega, \boldsymbol{\beta}) = \mathbf{F}_1(\boldsymbol{\beta}) - \omega^2 \mathbf{G}_1(\boldsymbol{\beta})$ of the amplitude-independent governing matrix). Differently, the third order perturbations are governed by two symmetric algebraic operators $\mathbf{F}_3(\boldsymbol{\beta}, \mathbf{a}_1, \mathbf{b}_1) = \mathbf{F}_3(\boldsymbol{\beta}, \mathbf{b}_1, \mathbf{a}_1)$ and $\mathbf{G}_3(\boldsymbol{\beta}, \mathbf{a}_1, \mathbf{b}_1) = \mathbf{G}_3(\boldsymbol{\beta}, \mathbf{b}_1, \mathbf{a}_1)$, which depend on the wavevector $\boldsymbol{\beta}$ but are also commutative quadratic functions of the harmonic amplitudes $\mathbf{a}_1$ and $\mathbf{b}_1$ (according to the expressions reported in Appendix B).

By exploiting the commutativity of the nonlinear operators, the companion eigenproblems can be solved by imposing the common characteristic equation $F(\omega, \boldsymbol{\beta}, \mathbf{a}_1, \mathbf{b}_1) = \det\left[\mathbf{F}_1(\boldsymbol{\beta}) - \omega^2 \mathbf{G}_1(\boldsymbol{\beta}) + \epsilon^2\left(\mathbf{F}_3(\boldsymbol{\beta}, \mathbf{a}_1, \mathbf{b}_1) - \omega^2 \mathbf{G}_3(\boldsymbol{\beta}, \mathbf{a}_1, \mathbf{b}_1)\right)\right] = 0$. According to the standard perturbation schemes for algebraic polynomial equations and in the absence of internal resonances [41,42], the characteristic equation is consistently satisfied – up to the third order – by nonlinear (amplitude-dependent) eigenvalues of the form $\varpi^2(\boldsymbol{\beta}, \mathbf{a}_1, \mathbf{b}_1) = \omega_1^2(\boldsymbol{\beta}) + \epsilon^2 \omega_3^2(\boldsymbol{\beta}, \mathbf{a}_1, \mathbf{b}_1)$. From the mathematical viewpoint, the second-order term $\omega_3^2(\boldsymbol{\beta}, \mathbf{a}_1, \mathbf{b}_1)$ is the nonlinear correction perturbing the

linear eigenvalue $\omega_1^2(\boldsymbol{\beta})$, valid for vanishing amplitudes (and thus coinciding with the solution of the linear eigenproblem). After some algebra, the nonlinear eigenvalues read

$$\varpi_a^2(\boldsymbol{\beta}, a_1, b_1) = \omega_a^2(\boldsymbol{\beta}) + \epsilon^2 \frac{\Lambda_a(\boldsymbol{\beta})}{\Gamma_a(\boldsymbol{\beta})} \left(a_1^2 + b_1^2\right) \tag{20}$$

$$\varpi_c^2(\boldsymbol{\beta}, c_1, d_1) = \omega_c^2(\boldsymbol{\beta}) + \epsilon^2 \frac{\Lambda_c(\boldsymbol{\beta})}{\Gamma_c(\boldsymbol{\beta})} \left(c_1^2 + d_1^2\right) \tag{21}$$

and can be interpreted as the (squared) *nonlinear wavefrequencies* of the polarized harmonic waves. Indeed, the linear wavefrequencies $\omega_a^2(\boldsymbol{\beta})$ and $\omega_c^2(\boldsymbol{\beta})$ are modified by the nonlinear corrections $\kappa_a(\boldsymbol{\beta})(a_1^2 + b_1^2)$ and $\kappa_c(\boldsymbol{\beta})(c_1^2 + d_1^2)$, depending quadratically on the linear amplitudes $\mathbf{a}_1 \pm \imath\mathbf{b}_1 = (a_1 \pm \imath b_1)\boldsymbol{\phi}_a$ (for u-polarization), or $\mathbf{a}_1 \pm \imath\mathbf{b}_1 = (c_1 \pm \imath d_1)\boldsymbol{\phi}_c$ (for v-polarization). The multipliers $\kappa_a(\boldsymbol{\beta}) = \Lambda_a(\boldsymbol{\beta})/\Gamma_a(\boldsymbol{\beta})$ and $\kappa_c(\boldsymbol{\beta}) = \Lambda_c(\boldsymbol{\beta})/\Gamma_c(\boldsymbol{\beta})$ of the quadratic amplitudes can be referred to as *effective nonlinearity coefficients*, depending on the numerators $\Lambda_a(\boldsymbol{\beta}) = \boldsymbol{\phi}_a^\top \mathbf{F}_3(\boldsymbol{\beta}, a_1\boldsymbol{\phi}_a, b_1\boldsymbol{\phi}_a)\boldsymbol{\phi}_a - \omega_a^2(\boldsymbol{\beta})\boldsymbol{\phi}_a^\top \mathbf{G}_3(\boldsymbol{\beta}, a_1\boldsymbol{\phi}_a, b_1\boldsymbol{\phi}_a)\boldsymbol{\phi}_a$ and $\Lambda_c(\boldsymbol{\beta}) = \boldsymbol{\phi}_c^\top \mathbf{F}_3(\boldsymbol{\beta}, c_1\boldsymbol{\phi}_a, d_1\boldsymbol{\phi}_c)\boldsymbol{\phi}_c - \omega_c^2(\boldsymbol{\beta})\boldsymbol{\phi}_c^\top \mathbf{G}_3(\boldsymbol{\beta}, c_1\boldsymbol{\phi}_c, d_1\boldsymbol{\phi}_c)\boldsymbol{\phi}_c$ and denominators $\Gamma_a = \boldsymbol{\phi}_a^\top \mathbf{G}_1(\boldsymbol{\beta})\boldsymbol{\phi}_a$ and $\Gamma_c = \boldsymbol{\phi}_c^\top \mathbf{G}_1(\boldsymbol{\beta})\boldsymbol{\phi}_c$.

From the mechanical viewpoint, the effective nonlinearity coefficients $\kappa_a(\boldsymbol{\beta})$ and $\kappa_c(\boldsymbol{\beta})$ can be given an interesting energy-based interpretation. Particularly, the coefficient $\kappa_a(\boldsymbol{\beta})$ characterizing the nonlinear wavefrequency $\varpi_a^2(\boldsymbol{\beta}, a_1, b_1)$ essentially depends on the numerator $\Lambda_a(\boldsymbol{\beta})$, which is the difference between two terms $\Lambda_a^e(\boldsymbol{\beta}) = \boldsymbol{\phi}_a^\top \mathbf{F}_3(\boldsymbol{\beta}, a_1\boldsymbol{\phi}_a, b_1\boldsymbol{\phi}_a)\boldsymbol{\phi}_a$ and $\Lambda_a^k(\boldsymbol{\beta}) = \omega_a^2(\boldsymbol{\beta})\boldsymbol{\phi}_a^\top \mathbf{G}_3(\boldsymbol{\beta}, a_1\boldsymbol{\phi}_a, b_1\boldsymbol{\phi}_a)\boldsymbol{\phi}_a$. Physically, the quantities $\Lambda_a^e(\boldsymbol{\beta})$ and $\Lambda_a^k(\boldsymbol{\beta})$ can be recognized as the works exerted on the same waveform $\boldsymbol{\phi}_a$ by the nonlinear elastic waveforce $\mathbf{F}_3(a_1\boldsymbol{\phi}_a, b_1\boldsymbol{\phi}_a)\boldsymbol{\phi}_a$ and inertial waveforce $\omega_a^2\mathbf{G}_3(a_1\boldsymbol{\phi}_a, b_1\boldsymbol{\phi}_a)\boldsymbol{\phi}_a$, respectively, related to the u-polarized wave with amplitude $\mathbf{a}_1 \pm \imath\mathbf{b}_1 = (a_1 \pm \imath b_1)\boldsymbol{\phi}_a$. Identical remarks can be pointed out for the nonlinearity coefficients $\kappa_c(\boldsymbol{\beta})$ characterizing the nonlinear wavefrequency $\varpi_c^2(\boldsymbol{\beta}, c_1, d_1)$. These findings are coherent with similar results achievable by different perturbation strategies (based on the multiple scale method), used to determine nonlinear frequencies of structural and microstructural systems [21,31,43].

Geometrically, the quadratic coefficients κ_a and κ_c define the curvatures of the parabolic curves describing the varying nonlinear wavefrequencies ϖ_a^2 and ϖ_c^2 for growing harmonic amplitudes $q_1^2 = a_1^2 + b_1^2$ and $p_1^2 = c_1^2 + d_1^2$, known as *backbone curves*. By noticing that denominators Γ_a and Γ_c must be strictly positive for physical reasons, from the physical interpretation follows that the elastic work prevailing over the inertial work ($\Lambda_a^e > \Lambda_a^k$ for ϖ_a^2 or $\Lambda_c^e > \Lambda_c^k$ for ϖ_c^2) determines positive curvatures, resulting in *hardening* behaviors of the backbone curve. On the contrary, the inertial work prevailing over the elastic work ($\Lambda_a^e < \Lambda_a^k$ for ϖ_a^2 or $\Lambda_c^e < \Lambda_c^k$ for ϖ_c^2) determines negative curvatures, resulting in *softening* behaviors of the backbone curve.

Parametric analyses show that the effective nonlinearity coefficients $\kappa_a(\boldsymbol{\beta})$ and $\kappa_c(\boldsymbol{\beta})$ attain positive values within two narrow regions $\mathscr{H}_a$ (purple) and $\mathscr{H}_c$ (pink) of the Brillouin zone $\mathcal{B}$ (Fig. 9a, b). Specifically, regions $\mathscr{H}_a$ and $\mathscr{H}_c$ cover nearly distinct and parameter-dependent sub-zones that closely and symmetrically surround the loci $\mathcal{B}_2$ and $\mathcal{B}_1$ (dashed gray lines), respectively, corresponding to the orthogonal axes of the wavevector plane. From the physical viewpoint, this major remark states that – for both possible wave polarizations – hardening behaviors occur only in transversal or quasi-transversal waves, whereas longitudinal and mixed waves tend to exhibit a softening behavior. As complementary remark, the qualitative transition from hardening to softening behaviors occurs smoothly at the frontiers $\mathscr{F}_a$ and $\mathscr{F}_c$ separating the regions $\mathscr{H}_a$ and $\mathscr{H}_c$ from the complementary regions $\mathscr{S}_a$ and $\mathscr{S}_c$ (gray). Frontiers $\mathscr{F}_a$ and $\mathscr{F}_c$ correspond to the wavevector loci in which the effective nonlinearity coefficients vanish ($\kappa_a(\boldsymbol{\beta}) = 0$ and $\kappa_c(\boldsymbol{\beta}) = 0$) and the wavefrequencies become independent of the oscillation amplitudes (within the limits of the third order asymptotic approximation). For both polarizations, the portion of Brillouin zone interested by hardening behaviors becomes significantly larger for growing values of the pantographic amplification angle α (Fig. 9c). On the contrary, the portion of Brillouin zone interested by hardening behaviors remain almost unaltered for varying values of the mass ratio ϱ^2 (Fig. 9d), except for a very small range of extremely low ϱ^2-values with limited technical significance. These remarks open the interesting possibility to consider the pantographic angle α as tuning parameter, which can be increased (or decreased) to govern the transition from softening to hardening behavior (or viceversa) for nonlinear waves propagating with certain wavevectors.

Wider parametric analyses of the coefficient $\kappa_a(\boldsymbol{\beta})$ within the region $\mathscr{S}_a$ (explored along the rectilinear locus $\mathcal{B}_3^S := \{\boldsymbol{\beta} : \beta_2 = 1/3\beta_1\}$ spanned by $\beta_1 = [0, \pi]$) highlight that stronger softening effects occur for short wavelengths (large wavenumbers β_1) or low pantographic amplification angles (Fig. 10a-d). Differently, parametric analyses within the complementary region $\mathscr{H}_a$ (explored along the rectilinear locus $\mathcal{B}_3^H := \{\boldsymbol{\beta} : \beta_1 = 1/3\beta_2\}$ spanned by $\beta_2 = [0, \pi]$) show that stronger hardening effects occur for mid-short wavelengths (mid-large wavenumbers β_2) and high pantographic amplification angles (Fig. 10e-h). From a general quantitative perspective, wavefrequency correction effects due to nonlinearities are larger in the softening region than in the hardening region. The highest softening effect (lowest nonlinearity coefficients) occurs at the largest wavenumbers β_1 and β_2 (shortest wavelengths), for the majority of the parameter range.

The nonlinear dispersion curves of the wavefrequencies $\varpi_a^2(\beta_1)$ and $\varpi_c^2(\beta_1)$ for increasing amplitudes q_1 and p_1 are compared for fixed mechanical parameters (ϱ^2, α) and wavevector $\boldsymbol{\beta}$ varying along the rectilinear locus $\mathcal{B}_3^S$. The strongly softening backbone curves of the higher wavefrequency $\varpi_a^2(\beta_1)$ for increasing amplitudes q_1 (red lines in Fig. 11a) and the slightly hardening backbone curves of the lower wavefrequency $\varpi_c^2(\beta_1)$ for increasing amplitudes p_1 (red lines in Fig. 11b) can be recognized. The nonlinear-to-linear wavefrequency ratios $\sigma_a^2 = \varpi_a^2/\omega_a^2 - 1$ and $\sigma_c^2 = \varpi_c^2/\omega_c^2 - 1$ are systematically negative (and monotonically decreasing with β_1) and positive (with a maximum close to $3/4\pi$), respectively (blue and red curves in Fig. 11c). The different behavior of the two nonlinear wavefrequencies $\varpi_a^2(\beta_1)$ and $\varpi_c^2(\beta_1)$ is coherent with the geometric position of the wavevector locus $\mathcal{B}_3^s$, which is fully contained in the softening region $\mathscr{S}_a$ and the hardening region $\mathscr{H}_c$ (Fig. 9a, b). It is interesting to remark that – along certain propagation directions – the qualitative behavior of a single nonlinear wavefrequency depends on the wavelength. Indeed, the nonlinear dispersion curve of

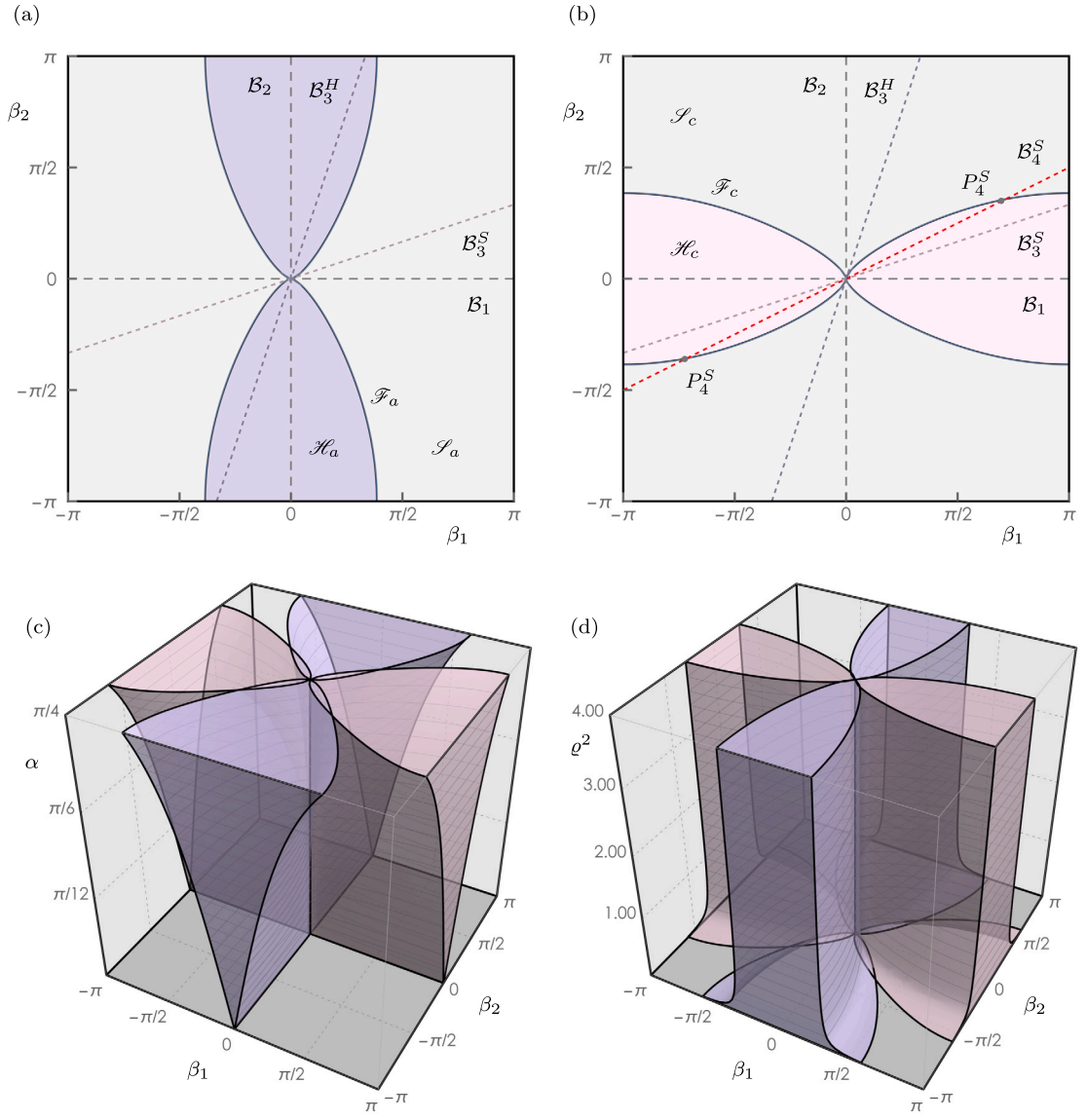

Fig. 9. Effective nonlinearity coefficients κ_a and κ_c of the nonlinear wavefrequencies ϖ_a^2 and ϖ_c^2 over the Brillouin zone $\mathcal{B}$ of the mechanical metamaterial (with mass ratio $\varrho^2 = 2$ and amplification angle $\alpha = \pi/5$): (a) hardening and softening regions $\mathscr{H}_a$ (purple) and $\mathscr{S}_a$ (gray) for κ_a, (b) hardening and softening regions $\mathscr{H}_c$ (pink) and $\mathscr{S}_c$ (gray) for κ_c, (c) hardening regions $\mathscr{H}_a$ (purple) and $\mathscr{H}_c$ (pink) versus varying pantographic amplification angle α, (d) hardening regions $\mathscr{H}_a$ (purple) and $\mathscr{H}_c$ (pink) versus varying mass ratio ϱ^2.

the wavefrequency $\varpi_c^2(\beta_1)$ along the rectilinear locus $\mathcal{B}_4^S := \{\boldsymbol{\beta} : \beta_2 = 1/2\beta_1\}$ (red dashed line in Fig. 9b) shows hardening behavior for long wavelengths (low wavenumbers β_1), while is characterized by softening behavior for short wavelengths (large wavenumbers β_1). The transition occurs at the critical points P_4^S (black dots), where the wavevector locus $\mathcal{B}_4^S$ intersects the frontier $\mathscr{F}_c$ separating the hardening region $\mathscr{H}_c$ from the softening region $\mathscr{S}_c$. Accordingly, point P_4^S identifies also the smooth change of sign (from positive to negative) of the wavefrequency ratio σ_c^2 (dashed red curve in Fig. 11c).

Finally, the evanescent nonlinear wavefrequency $\varpi_a^2(\beta_2)$ emergent from the zero wavefrequency of linear kinematic (floppy) modes can be determined for wavevectors $\boldsymbol{\beta} \in \mathcal{B}_2$ (Fig. 12a). The backbone curves for growing oscillation amplitudes p_1 (red lines) show a systematic hardening behavior, as expected for physical reasons (for the sake of frequency positivity and also consistently with the geometric position of the wavevector locus $\mathcal{B}_2$, which is fully contained in the region $\mathscr{H}_a$). Independently of the oscillation amplitude, the essentially nonlinear wavefrequencies become larger for shorter wavelengths (larger wavenumbers β_2). Parametric analyses for a fixed oscillation amplitude show how larger hardening effects systematically occur for lower pantographic amplification angles α and smaller mass ratios ϱ^2 for all wavenumbers β_2 (Fig. 9b). The rich scenario of nonlinear dynamic phenomena generated by essentially nonlinear stiffnesses of kinematically propagating waves opens interesting possibilities for the spectral design of ultra-low frequency metafilters, as well as for wideband vibration control via targeted energy transfers [44].

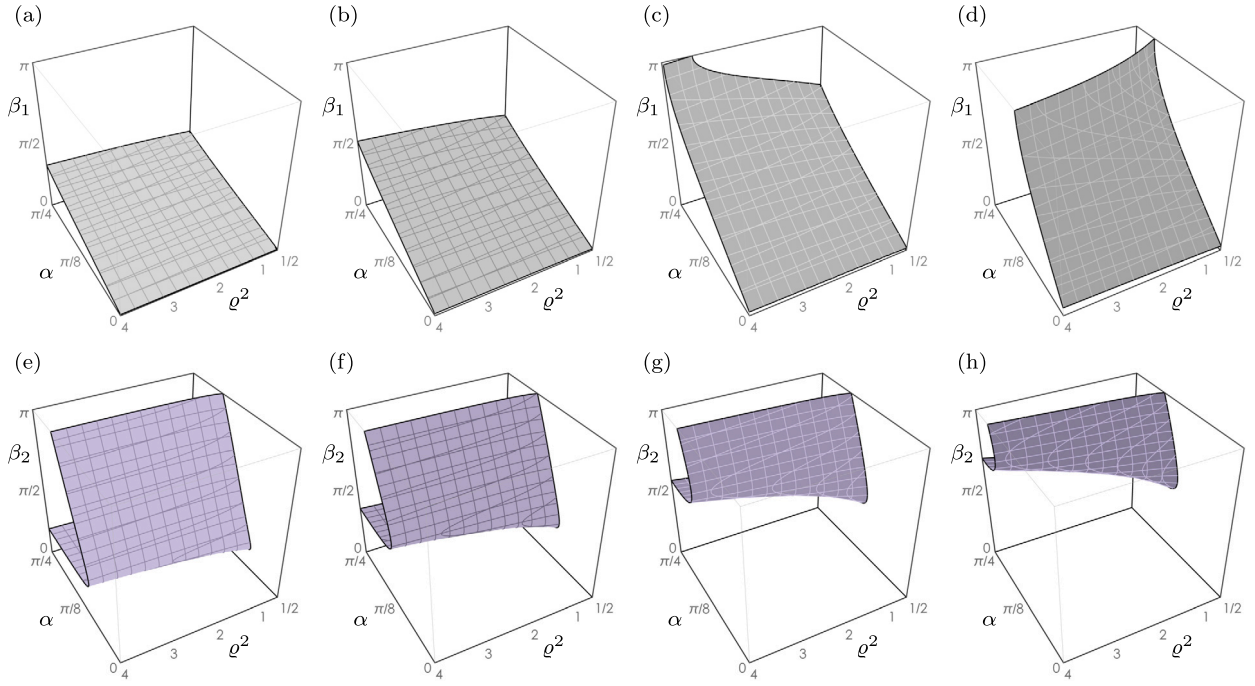

Fig. 10. Effective nonlinearity coefficient κ_a of the nonlinear wavefrequency ϖ_a^2. Upper row (gray scale): negative values along the locus $\mathcal{B}_3^S$ of the softening region $\mathcal{S}_a$: (a) $\kappa_a = -1/10$, (b) $\kappa_a = -1$, (c) $\kappa_a = -10$, (d) $\kappa_a = -100$. Lower row (purple scale): positive values along the locus $\mathcal{B}_3^H$ of the hardening region $\mathcal{H}_a$: (e) $\kappa_a = 1/100$, (f) $\kappa_a = 1/10$, (g) $\kappa_a = 1$, (h) $\kappa_a = 2$.

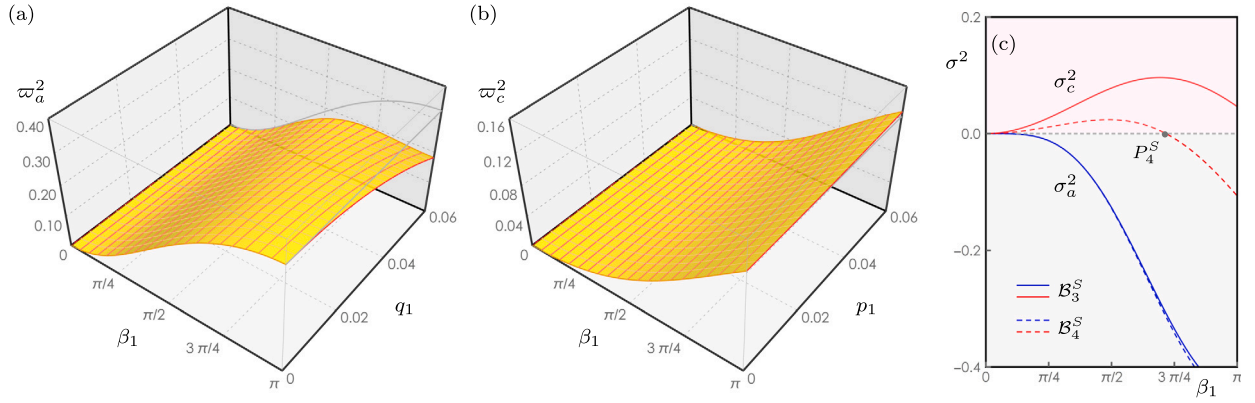

Fig. 11. Nonlinear dispersion curves (yellow) and backbone curves (red) versus linear wavefrequencies (gray) of the mechanical metamaterial (with mass ratio $\varrho^2 = 2$ and amplification angle $\alpha = \pi/5$): (a) softening wavefrequency $\varpi_a^2(\beta_1)$ for increasing amplitudes q_1, (b) hardening wavefrequency $\varpi_c^2(\beta_1)$ for increasing amplitudes p_1, (c) wavefrequency ratios for wavevector loci $\mathcal{B}_3^S$ (red curves) and $\mathcal{B}_4^S$ (dashed red curve).

4. Multi-harmonic wave response

Once the amplitudes of the superharmonic components are determined as a function of the undetermined amplitudes of the harmonic component, the multi-harmonic wave response can be reconstructed in the time domain up to the third order ($m = 3$). By adopting the convenient trigonometric form of the Fourier series, the reconstructed response reads

$$\mathbf{u}(\mathbf{z},\tau) = \mathbf{a}_0 + \sum_{n=1}^{m} \epsilon^n \left[2\mathbf{a}_n \cos(\boldsymbol{\beta}\cdot\mathbf{z} + n\omega\tau) + 2\mathbf{b}_n \sin(\boldsymbol{\beta}\cdot\mathbf{z} + n\omega\tau) \right] \tag{22}$$

where the independent amplitudes $\mathbf{a}_n$ and $\mathbf{b}_n$ can be recognized to multiply orthogonal (in quadrature) time-dependent terms of the trigonometric series at the site $\mathbf{z}$. The quasi-static amplitude $\mathbf{a}_0$ is unessential for the analysis of the dynamic response and can be assumed null for the sake of simplicity. The leading amplitudes $\mathbf{a}_1 = (a_1, c_1)$ and $\mathbf{b}_1 = (b_1, d_1)$ can be determined analytically by imposing initial conditions (at time $\tau = 0$), if ϵ-order displacement and velocity are assigned to a certain site. Coherently with the hypotheses assumed for the analyses in the frequency domain, only initial conditions that generate perfect u-polarization or v-polarization in

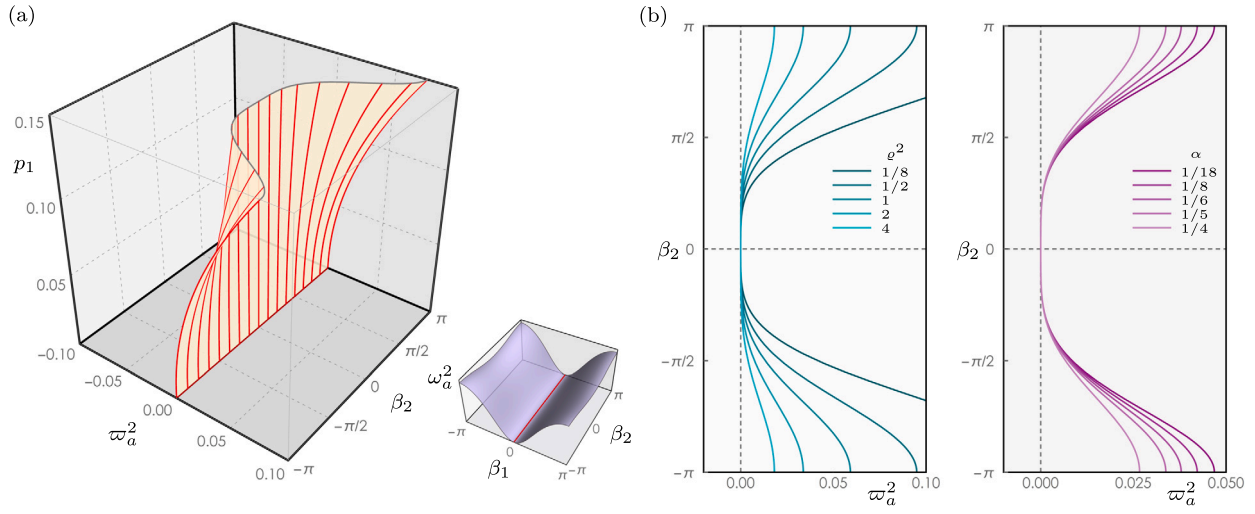

Fig. 12. Evanescent nonlinear wavefrequency $\varpi_a^2(\beta_2)$ of floppy modes: (a) backbone curves for the mechanical metamaterial with mass ratio $\varrho^2 = 2$ and amplification angle $\alpha = \pi/5$, (b) nonlinear wavefrequencies $\varpi_a^2(\beta_2)$ for different mass ratios ϱ^2 (and fixed amplification angle $\alpha = \pi/5$) or different amplification angles α (and fixed mass ratio $\varrho^2 = 2$).

the linear response are considered. Therefore, the higher order amplitudes are determined as $\mathbf{a}_2 = \mathbf{H}(2\omega,\boldsymbol{\beta})^{-1}\mathbf{f}_2(\omega,\boldsymbol{\beta},\mathbf{a}_1,\mathbf{b}_1)$, $\mathbf{b}_2 = \mathbf{H}(2\omega,\boldsymbol{\beta})^{-1}\mathbf{g}_2(\omega,\boldsymbol{\beta},\mathbf{a}_1,\mathbf{b}_1)$ and $\mathbf{a}_3 = \mathbf{H}(3\omega,\boldsymbol{\beta})^{-1}\mathbf{f}_3(\omega,\boldsymbol{\beta},\mathbf{a}_1,\mathbf{b}_1,\mathbf{a}_2,\mathbf{b}_2)$, $\mathbf{b}_3 = \mathbf{H}(3\omega,\boldsymbol{\beta})^{-1}\mathbf{g}_3(\omega,\boldsymbol{\beta},\mathbf{a}_1,\mathbf{b}_1,\mathbf{a}_2,\mathbf{b}_2)$. Given a certain parameter combination, the reconstruction of the multi-harmonic solution requires checking a posteriori the postulated ordering of the harmonic components, that is necessary for the mathematical consistency of the perturbation results. As an alternative to a posteriori checking of the reconstructed solutions, a viable parametric strategy to determine a priori the consistency limits of the perturbation scheme, in terms of maximal leading amplitudes, is outlined in [22] for a one-dimensional metamaterial traveled by longitudinal waves. The leading amplitudes are also required to satisfy the inequalities $4\left[a_1(1-\cos\beta_1)+b_1\sin\beta_1\right]\cos(\omega\tau)+4\left[b_1(1-\cos\beta_1)-a_1\sin\beta_1\right]\sin(\omega\tau) < \sec^2(\alpha)-1$ and $4\left[c_1(1-\cos\beta_2)+d_1\sin\beta_2\right]\cos(\omega\tau)+4\left[d_1(1-\cos\beta_2)-c_1\sin\beta_2\right]\sin(\omega\tau) < \sec^2(\alpha)-1$, according to a first-order approximation of the validity conditions imposed by the inextensibility of the pantographic arms.

The multi-harmonic wave response $\mathbf{u}(\mathbf{z},\tau)$ at the origin (corresponding to site vector $\mathbf{z} = (0,0)$) is analyzed in the cases of linearly u-polarized waves (Fig. 13) and linearly v-polarized waves (Fig. 14), propagating with wavevector $\boldsymbol{\beta} = (5/6\pi, 1/2\pi)$ through the particular mechanical metamaterial characterized by amplification angle $\alpha = \pi/5$ and mass ratio $\varrho^2 = 2$. Considering first u-polarized waves, the time-dependent response is represented within the *polarization phase plane* $\mathcal{P}_u = \{u,\dot{u}\}$ of the *dragging* variable $u(\tau)$ in Fig. 13a, within the *depolarization phase plane* $\mathcal{D}_u = \{v,\dot{v}\}$ of the *dragged* variable $v(\tau)$ in Fig. 13b, and within the extended phase space $\mathcal{S}_u = \{u,\dot{u},v\}$ in Fig. 13c. Considering instead v-polarized waves, the time-dependent response is represented within the *polarization phase plane* $\mathcal{P}_v = \{v,\dot{v}\}$ of the *dragging* variable $v(\tau)$ in Fig. 14b, within the *depolarization phase plane* $\mathcal{D}_v = \{u,\dot{u}\}$ of the *dragged* variable $u(\tau)$ in Fig. 14a, and within the extended phase space $\mathcal{S}_v = \{v,\dot{v},u\}$ in Fig. 14c. Different initial conditions are properly assigned to provide leading amplitudes $\mathbf{a}_1 = (0.02,0)$ and $\mathbf{b}_1 = (0.02,0)$ for u-polarized waves, or $\mathbf{a}_1 = (0,0.03)$ and $\mathbf{b}_1 = (0,0.03)$ for v-polarized waves. The leading amplitudes generated by all the initial conditions satisfy the inequalities required for the solution validity. Specifically, for the selected parameters and initial conditions, the time-dependent left-hand terms of the non-trivial inequalities attain the maximum values 0.218 and 0.240, which are lower than the right-hand threshold 0.528. For both polarizations, three different solutions are illustrated, representing the mono-harmonic linear response (gray curves), the three-harmonic $(\omega,2\omega,3\omega)$ response obtained from Section 3.2 without considering the nonlinear correction to the harmonic contribution (blue curves), and the three-harmonic response obtained including the nonlinear frequency correction at the third order described in Section 3.3 (orange curves).

As primary remark, the phenomenon of nonlinear depolarization can be recognized by comparing the rest position of the linear harmonic response (gray dot) with the orbits of the purely superharmonic response (blue and orange curves) for the dragged variables v (for the u-polarized wave) and u (for the v-polarized wave) in Figs. 13b and 14a, respectively. In the three-dimensional phase spaces $\mathcal{S}_u$ and $\mathcal{S}_v$, the linear harmonic responses of the u-polarized and v-polarized waves describe planar orbits (gray curves in Fig. 13c and 14c). Here, the primary effect of the nonlinear depolarization is a significant loss of planarity in the orbits described by the superharmonic response (non-planar blue and orange curves). As secondary remark, the comparison between the harmonic solutions (gray) and multi-harmonic solutions (blue) highlights the distortion effects produced by the superharmonic $(2\omega,3\omega)$ components on the orbits in all the phase planes. Consistently with the perturbation scheme, the superharmonic components have smaller amplitudes than the leading harmonic components. Consequently, the superharmonic distortion effects cause: (i) a slight but evident loss of symmetry in the elliptic (symmetric) orbits of the leading harmonic components characterizing the dragging variables in the polarization phase planes $\mathcal{P}_u$ and $\mathcal{P}_v$ (Figs. 13a and 14b), and (ii) the arise of a double loop featuring the small-amplitude periodic orbits of the dragged variables in the depolarization phase planes $\mathcal{D}_u$ and $\mathcal{D}_v$ (Figs. 13b and 14a). As complementary remark, accounting for the third-order nonlinear correction to the harmonic component does not imply qualitative modifications of the dynamic scenario,

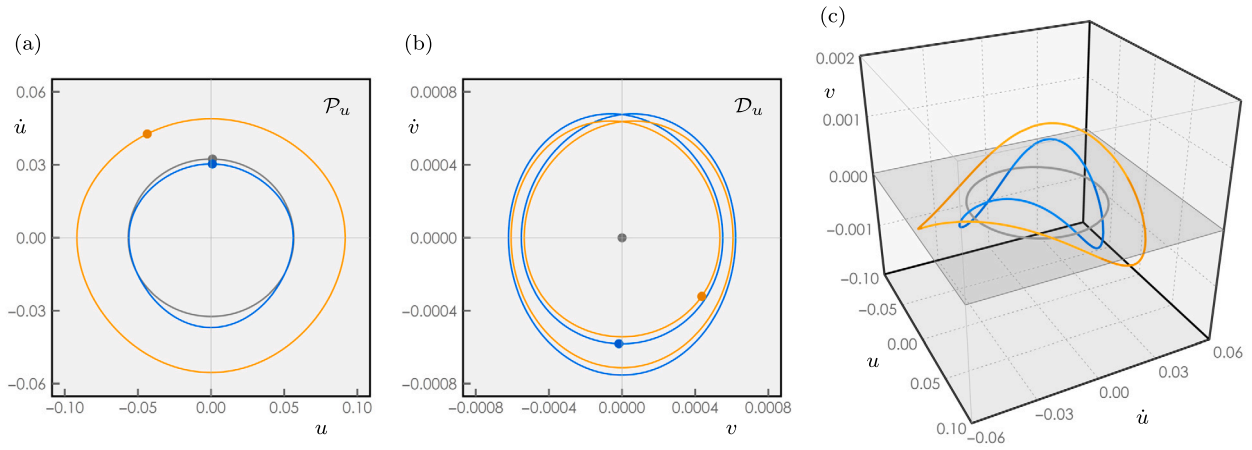

Fig. 13. Time-domain response (at site $\mathbf{z} = \mathbf{0}$) of the mechanical metamaterial with parameters $\alpha = \pi/5$ and $\varrho^2 = 2$ generated by the linearly u-polarized waves $\mathbf{u}(\mathbf{z}, \tau)$ propagating with wavevector $\boldsymbol{\beta} = (5/6\pi, 1/2\pi)$. Comparison among the linear harmonic solution (gray) and the nonlinear multi-harmonic solutions without (blue) and with (orange) the nonlinear frequency correction in: (a) the polarization phase plane $\mathcal{P}_u$, (b) the depolarization phase plane $\mathcal{D}_u$, (c) the phase space $\mathcal{S}_u$.

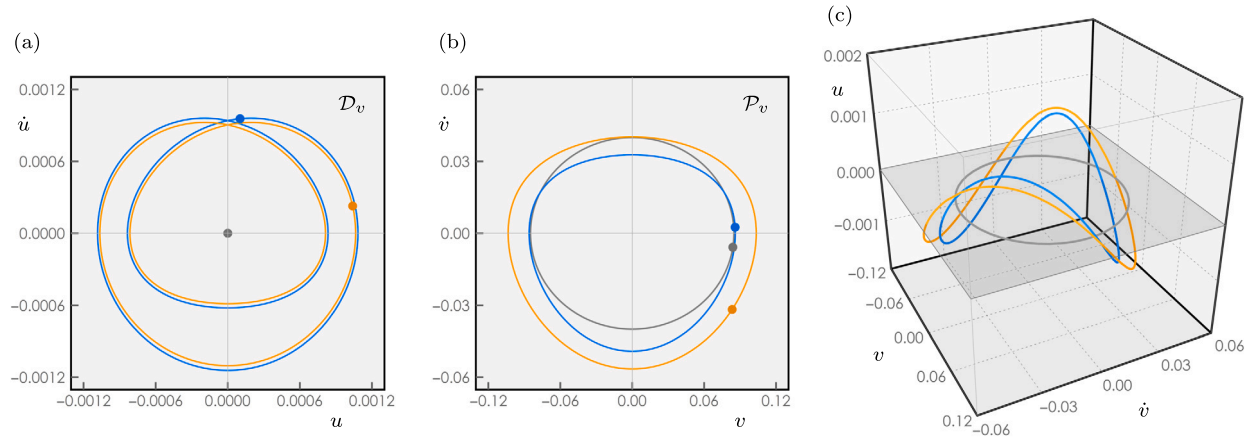

Fig. 14. Time-domain response (at site $\mathbf{z} = \mathbf{0}$) of the mechanical metamaterial with parameters $\alpha = \pi/5$ and $\varrho^2 = 2$ generated by the linearly v-polarized waves $\mathbf{u}(\mathbf{z}, \tau)$ propagating with wavevector $\boldsymbol{\beta} = (5/6\pi, 1/2\pi)$. Comparison among the linear harmonic solution (gray) and the nonlinear multi-harmonic solutions without (blue) and with (orange) the nonlinear frequency correction in: (a) the depolarization phase plane $\mathcal{D}_v$, (b) the polarization phase plane $\mathcal{P}_v$, (c) the phase space $\mathcal{S}_v$.

but determines quantitative modifications in the response, essentially consisting of a pronounced increase in the overall response amplitudes. The comparison between the uncorrected and corrected responses highlights that the amplitude increase is more evident in the dragging variables (orange versus blue orbits in Figs. 13a and 14b), while is less significant – although appreciable – in the dragged variables (Figs. 13b and 14a), whose purely superharmonic response modifications are related to the third order nonlinear frequency correction only. As final remark, the solution periodicity is confirmed by the single point representation of the Poincaré map (blue and orange dots) in the phase planes.

5. Conclusions

A two-dimensional microstructured lattice is proposed as minimal physical-mathematical model describing the free undamped dynamics of a planar mechanical metamaterial with inertia amplification. The metamaterial microstructure is characterized by an infinite periodic array of massive point particles (atoms). Quartets of adjacent atoms are interconnected by rhombic microtruss systems, elastically stiffened along the principal diagonal. The quadrilateral geometry of each microtruss system realizes a local lever mechanism that exploits the eccentric masses of secondary atoms (aligned with the smaller diagonal) to pantographically amplify the inertial properties of the principal atoms (aligned with the larger diagonal). The mechanical properties of the metamaterial are fully described by the pantographic amplification angle and the nondimensional mass ratio between secondary and primary atoms. Imposing the axial indeformability of the pantograph arms allows to reduce the space of configuration variables to the in-plane displacements of the principal atoms. Therefore, by following the principles of Lagrangian mechanics, the second-order ordinary differential (in time), second-order difference (in space) equations of motion are derived, in the framework of a finite kinematic formulation. Considering the neighborhood of the rest configuration, the fully nonlinear equations of motion are consistently approximated by expanding the

configuration variables in polynomial series. Neglecting higher-order terms, quadratic and cubic nonlinearities of both inertial and elastic nature are found to coexist. The former are generated by the indeformability constraints of the microtrusses, whereas the latter follow from finite elongations of the principal diagonal in the rhombic microtruss mechanisms.

In the absence of analytical exact solutions, the nonlinear equations of motion are solved asymptotically by employing a suited perturbation method. Specifically, real-valued multi-harmonic solutions are sought for in the form of a two-dimensional exponential Fourier series that describes periodic planar waves oscillating harmonically – in time – with a leading wavefrequency (harmonic component) and its integer multiples (superharmonic components), while propagating – in space – with a real-valued wavevector. According to the perturbation scheme, the amplitudes of superharmonic components are ordered to increasing integer powers of a small bookkeeping parameter. By adopting this methodological strategy, the nonlinear equations of motion are transformed into an ordered hierarchy of algebraic perturbation equations.

The first order set of perturbation equations states the spectral eigenproblem governing the linear dispersion relation for the metamaterial. The analytical eigensolution returns a pair of linear wavefrequencies, corresponding to linear waveforms that are perfectly polarized in one or the other configuration variables. From the qualitative viewpoint, parametric analyses show that the two linear wavefrequencies cover the same low-frequency pass band. Interestingly, internal 1:1, 1:2 and 1:3 resonance conditions occur for analytically determinable loci of wavevectors in the first Brillouin zone. Analyzing the vector fields of group velocities discloses also the dispersive nature of the metamaterial. From the quantitative viewpoint, parametric analyses of the dispersion curves reveal that larger pass-bandwidths can be achieved by increasing the amplification angle or by reducing the mass ratio. Focusing on the polarized waveforms, the eigensolution discloses that longitudinal (pressure), transversal (shear) and mixed (pressure-shear) waves can exist in the linear regime, depending on the propagation direction. As remarkable physical phenomenon, pure shear waves propagate along the principal directions as pure kinematic modes (*floppy modes* with evanescent wavefrequency) for all the wavelengths. This peculiar dynamic behavior can be mechanically ascribed to the essentially nonlinear transversal stiffness of the kinematically indeterminate microtruss systems.

The second and third order sets of perturbation equations determine coupled systems of linear equations that return the amplitudes of the superharmonic wave components generated by a selected first order harmonic solution (generating solution). Specifically, the amplitudes of the superharmonic components oscillating with double (second superharmonic) and triple (third superharmonic) multiples of the linear wavefrequency are analytically determined, by assuming a mono-harmonic perfectly polarized wave as generating solution in the absence of internal resonances. From a qualitative perspective, the amplitudes of the second and third superharmonic components are found to depend quadratically and cubically on the amplitude of the linear harmonic component, as expected. The analytical functions of the second and third superharmonic amplitudes are found to describe saddle surfaces with negative Gaussian curvature in the space of harmonic amplitudes. Interestingly, combinations of harmonic linear amplitudes that do not generate superharmonic amplitudes exist, independently of the propagation wavelengths and mechanical parameters. As a noteworthy physical phenomenon, the generation of superharmonic components determines the loss of the perfect polarization (*superharmonic depolarization*) characterizing the generating linear solution. Parametric analyses show that the concurrent effects of nonlinear depolarization caused by the second and third superharmonic components are maximized by large but different amplification angles.

The third order perturbation equations also generate a nonlinear eigenproblem, governing the characteristic dependence of the harmonic wavefrequencies on the oscillation amplitude of the linear waveforms. In the absence of internal resonances, both nonlinear wavefrequencies are analytically determined to depend quadratically on the oscillation amplitude. The effective nonlinearity coefficients ruling the amplitude-dependent increment (*hardening*) or decrement (*softening*) of the wavefrequencies have been given an interesting energetic interpretation, based on the work done by the nonlinear waveforces into the linear waveforms. The hardening and softening regions in the parameter space are determined analytically, and the effects of the mechanical parameters on the effective nonlinearity coefficients are discussed quantitatively. As general remark, pressure waves and shear waves are found to exhibit a systematic softening and hardening behavior, respectively. Remarkably, the nonlinear behavior of mixed waves within a small range of propagation directions changes from softening to hardening (and viceversa), depending on the wavelength. Finally, the emergence of the evanescent nonlinear wavefrequencies of kinematic shear waveforms (floppy modes with essentially nonlinear stiffness and null linear wavefrequency) is parametrically described.

CRediT authorship contribution statement

Marco Lepidi: Writing – review & editing, Writing – original draft, Validation, Supervision, Methodology, Investigation, Formal analysis, Conceptualization. **Valeria Settimi:** Writing – review & editing, Writing – original draft, Validation, Supervision, Methodology, Investigation, Formal analysis, Conceptualization.

Declaration of competing interest

The authors declare that they have no known competing financial interests or personal relationships that could have appeared to influence the work reported in this paper.

Acknowledgements

VS acknowledges the financial support of European Union - Next Generation EU, in the framework of the project PRIN 2022 M4-C2-I.1.1, 2022TH5HC2, Engineered basements for vibration protection of artworks and strategic sensitive equipment.

Appendix A. Nonlinear equations of motion

A.1. Elastic nonlinearities

The quadratic elastic terms in the nonlinear equations (9), (10) are

$$\kappa_2^u = v_{ij}(u_j^+ - u_j^- + v_i^+ - v_i^-) + u_{ij}(v_j^+ - v_j^-) + u_j^- v_j^- - u_j^+ v_j^+ + \tfrac{1}{2}\left[(v_i^-)^2 - (v_i^+)^2\right] \tag{A.1}$$

$$\kappa_2^v = u_{ij}(u_j^+ - u_j^- + v_i^+ - v_i^-) + v_{ij}(u_i^+ - u_i^-) + u_i^- v_i^- - u_i^+ v_i^+ + \tfrac{1}{2}\left[(u_j^-)^2 - (u_j^+)^2\right] \tag{A.2}$$

where, remarkably, terms u_{ij}^2 and v_{ij}^2 are absent. The cubic elastic terms are

$$\begin{aligned}\kappa_3^u = {} & u_{ij}^3 - \tfrac{3}{2}u_{ij}^2(u_j^- + u_j^+) + v_{ij}^2(u_i^- + u_i^+ + u_j^- + u_j^+) - 2u_{ij}v_{ij}(2v_{ij} - v_i^- - v_i^+ - v_j^- - v_j^+) + \\ & - u_{ij}\left[(v_i^-)^2 + (v_i^+)^2 + (v_j^-)^2 + (v_j^+)^2 - \tfrac{3}{2}\left((u_j^-)^2 + (u_j^+)^2\right)\right] - 2v_{ij}(u_i^- v_i^- + u_i^+ v_i^+ + u_j^- v_j^- + u_j^+ v_j^+) + \\ & + u_i^-(v_i^-)^2 + u_i^+(v_i^+)^2 + u_j^-(v_j^-)^2 + u_j^+(v_j^+)^2 - \tfrac{1}{2}\left((u_j^-)^3 + (u_j^+)^3\right)\end{aligned} \tag{A.3}$$

$$\begin{aligned}\kappa_3^v = {} & v_{ij}^3 - \tfrac{3}{2}v_{ij}^2(v_i^- + v_i^+) + u_{ij}^2(v_i^- + v_i^+ + v_j^- + v_j^+) - 2u_{ij}v_{ij}(2u_{ij} - u_i^- - u_i^+ - u_j^- - u_j^+) + \\ & - v_{ij}\left[(u_i^-)^2 + (u_i^+)^2 + (u_j^-)^2 + (u_j^+)^2 - \tfrac{3}{2}\left((v_i^-)^2 + (v_i^+)^2\right)\right] - 2u_{ij}(u_i^- v_i^- + u_i^+ v_i^+ + u_j^- v_j^- + u_j^+ v_j^+) + \\ & + v_i^-(u_i^-)^2 + v_i^+(u_i^+)^2 + v_j^-(u_j^-)^2 + v_j^+(u_j^+)^2 - \tfrac{1}{2}\left((v_i^-)^3 + (v_i^+)^3\right)\end{aligned} \tag{A.4}$$

where all the coupling terms are present, except $u_{ij}^2 v_{ij}$ and v_{ij}^3 (in κ_3^u) and $v_{ij}^2 u_{ij}$ and u_{ij}^3 (in κ_3^v).

A.2. Inertial nonlinearities

The quadratic inertial terms in the nonlinear equations (9), (10) are

$$\begin{aligned}\mu_2^u = {} & c_{21}\left[2\dot v_{ij}(\dot v_i^+ - \dot v_i^-) - (\dot v_i^+)^2 + (\dot v_i^-)^2\right] + \\ & + c_{22}\left[2u_{ij}(\ddot u_i^+ - \ddot u_i^-) + 2\dot u_{ij}(\dot u_i^+ - \dot u_i^-) + 2\ddot u_{ij}(u_i^+ - u_i^-) + 2\ddot u_i^- u_i^- - 2\ddot u_i^+ u_i^+ + (\dot u_i^-)^2 - (\dot u_i^+)^2\right] + \\ & + c_{23}\left[\ddot v_{ij}(v_i^+ - v_i^- + u_j^+ - u_j^-) + v_{ij}(\ddot v_i^+ - \ddot v_i^-) + u_{ij}(\ddot v_j^+ - \ddot v_j^-) + \ddot v_i^- v_i^- - \ddot v_i^+ v_i^+ + \ddot v_j^- u_j^- - \ddot v_j^+ u_j^+\right] + \\ & + c_{24}\left[\ddot u_{ij}(v_j^- - v_j^+) + v_{ij}(\ddot u_j^- - \ddot u_j^+) + \dot u_{ij}(\dot v_j^- - \dot v_j^+) + \dot v_{ij}(\dot u_j^- - \dot u_j^+) - \ddot u_j^- v_j^- + \ddot u_j^+ v_j^+ - \dot u_j^- \dot v_j^- + \dot u_j^+ \dot v_j^+\right]\end{aligned} \tag{A.5}$$

$$\begin{aligned}\mu_2^v = {} & c_{21}\left[2\dot u_{ij}(\dot u_j^+ - \dot u_j^-) - (\dot u_j^+)^2 + (\dot u_j^-)^2\right] + \\ & + c_{22}\left[2v_{ij}(\ddot v_j^+ - \ddot v_j^-) + 2\dot v_{ij}(\dot v_j^+ - \dot v_j^-) + 2\ddot v_{ij}(v_j^+ - v_j^-) + 2\ddot v_j^- v_j^- - 2\ddot v_j^+ v_j^+ + (\dot v_j^-)^2 - (\dot v_j^+)^2\right] + \\ & + c_{23}\left[\ddot u_{ij}(v_i^+ - v_i^- + u_j^+ - u_j^-) + u_{ij}(\ddot u_j^+ - \ddot u_j^-) + v_{ij}(\ddot u_i^+ - \ddot u_i^-) + \ddot u_j^- u_j^- - \ddot u_j^+ u_j^+ + \ddot u_i^- v_i^- - \ddot u_i^+ v_i^+\right] + \\ & + c_{24}\left[\ddot v_{ij}(u_i^- - u_i^+) + u_{ij}(\ddot v_i^- - \ddot v_i^+) + \dot v_{ij}(\dot u_i^- - \dot u_i^+) + \dot u_{ij}(\dot v_i^- - \dot v_i^+) - \ddot v_i^- u_i^- + \ddot v_i^+ u_i^+ - \dot u_i^- \dot v_i^- + \dot u_i^+ \dot v_i^+\right]\end{aligned} \tag{A.6}$$

and the cubic inertial terms are

$$\begin{aligned}\mu_3^u = {} & c_{301}v_{ij}(\ddot u_{ij}v_{ij} + 2\dot u_{ij}\dot v_{ij}) + c_{302}\dot v_{ij}^2 u_{ij} + c_{303}u_{ij}\left(\ddot u_{ij}u_{ij} + \dot u_{ij}^2\right) + \\ & + c_{304}\left[u_{ij}\left((\dot v_i^-)^2 + (\dot v_i^+)^2 - 2\dot v_{ij}(\dot v_i^- + \dot v_i^+)\right) + 2\dot v_{ij}(\dot v_i^- u_i^- + \dot v_i^+ u_i^+) - \dot v_{ij}^2(u_i^- + u_i^+) - u_i^-(\dot v_i^-)^2 - u_i^+(\dot v_i^+)^2\right] + \\ & + c_{305}\left[\ddot u_{ij}\left((v_j^-)^2 + (v_j^+)^2 - 2v_{ij}(v_j^- + v_j^+)\right) - 2\dot u_{ij}\left(\dot v_{ij}(v_j^- + v_j^+) + v_{ij}(\dot v_j^- + \dot v_j^+) - \dot v_j^- v_j^- - \dot v_j^+ v_j^+\right)\right] + \\ & - c_{305}\left[v_{ij}^2(\ddot u_j^- + \ddot u_j^+) + 2v_{ij}\left(\dot v_{ij}(\dot u_j^- + \dot u_j^+) - \ddot u_j^- v_j^- - \ddot u_j^+ v_j^+ - \dot u_j^- \dot v_j^- - \dot u_j^+ \dot v_j^+\right)\right] + \\ & + c_{305}\left[2\dot v_{ij}(\dot u_j^- v_j^- + \dot u_j^+ v_j^+) - v_j^-(\ddot u_j^- v_j^- + 2\dot u_j^- \dot v_j^-) - v_j^+(\ddot u_j^+ v_j^+ + 2\dot u_j^+ \dot v_j^+)\right] + \\ & + c_{306}\left[u_{ij}^2(\ddot u_j^- + \ddot u_j^+) + u_{ij}\left(2\ddot u_{ij}(u_j^- + u_j^+) + 2\dot u_{ij}(\dot u_j^- + \dot u_j^+) - 2\ddot u_j^- u_j^- - 2\ddot u_j^+ u_j^+ - (\dot u_j^-)^2 - (\dot u_j^+)^2\right)\right] + \\ & + c_{306}\left[\dot u_{ij}^2(u_j^- + u_j^+) - 2\dot u_{ij}(\dot u_j^- u_j^- + \dot u_j^+ u_j^+) - \ddot u_{ij}\left((u_j^-)^2 + (u_j^+)^2\right) + u_j^-\left(\ddot u_j^- u_j^- + (\dot u_j^-)^2\right) + u_j^+\left(\ddot u_j^+ u_j^+ + (\dot u_j^+)^2\right)\right] + \\ & - c_{307}\left[v_{ij}^2(\ddot u_i^- + \ddot u_i^+) + 2v_{ij}\left(\dot v_{ij}(\dot u_i^- + \dot u_i^+) - \ddot u_i^- v_i^- - \ddot u_i^+ v_i^+ - \dot u_i^- \dot v_i^- - \dot u_i^+ \dot v_i^+\right) - 2\dot v_{ij}(\dot u_i^- v_i^- + \dot u_i^+ v_i^+)\right] + \\ & - c_{307}\left[2\dot u_{ij}(\dot v_{ij}(v_i^- + v_i^+) + v_{ij}(\dot v_i^- + \dot v_i^+) - \dot v_i^- v_i^- - \dot v_i^+ v_i^+) - \ddot u_{ij}\left((v_i^-)^2 - 2v_{ij}(v_i^- + v_i^+) + (v_i^+)^2\right)\right] + \\ & - c_{307}\left[v_i^-(\ddot u_i^- v_i^- + 2\dot u_i^- \dot v_i^-) + v_i^+(\ddot u_i^+ v_i^+ + 2\dot u_i^+ \dot v_i^+)\right] + \\ & + c_{308}\left[u_{ij}\left((\dot v_j^-)^2 - 2\dot v_{ij}(\dot v_j^- + \dot v_j^+) + (\dot v_j^+)^2\right) - \dot v_{ij}^2(u_j^- + u_j^+) + 2\dot v_{ij}(\dot v_j^- u_j^- + \dot v_j^+ u_j^+) - u_j^-(\dot v_j^-)^2 - u_j^+(\dot v_j^+)^2\right] + \\ & + c_{309}\left[v_{ij}\left(\ddot v_i^- u_i^- + \ddot v_i^+ u_i^+ + \ddot v_j^- u_j^- + \ddot v_j^+ u_j^+ - \ddot v_{ij}(u_i^- + u_i^+ + u_j^- + u_j^+)\right) + \ddot v_{ij}(u_i^- v_i^- + u_i^+ v_i^+ + u_j^- v_j^- + u_j^+ v_j^+)\right] + \\ & + c_{309}\left[u_{ij}\left(v_{ij}(4\ddot v_{ij} - \ddot v_i^- - \ddot v_i^+ - \ddot v_j^- - \ddot v_j^+) - \ddot v_{ij}(v_i^- + v_i^+ + v_j^- + v_j^+) + \ddot v_i^- v_i^- + \ddot v_i^+ v_i^+ + \ddot v_j^- v_j^- + \ddot v_j^+ v_j^+\right)\right] + \\ & - c_{309}\left[\ddot v_i^- u_i^- v_i^- + \ddot v_i^+ u_i^+ v_i^+ + \ddot v_j^- u_j^- v_j^- + \ddot v_j^+ u_j^+ v_j^+\right] +\end{aligned} \tag{A.7}$$

$$
\begin{aligned}
&- c_{310}\left[u_{ij}^2(\ddot{u}_i^- + \ddot{u}_i^+) + u_{ij}\left(2\ddot{u}_{ij}(u_i^- + u_i^+) + 2\dot{u}_{ij}(\dot{u}_i^- + \dot{u}_i^+) - 2\ddot{u}_i^- u_i^- - 2\ddot{u}_i^+ u_i^+ - (\dot{u}_i^-)^2 - (\dot{u}_i^+)^2\right)\right] + \\
&+ c_{310}\left[\ddot{u}_{ij}\left((u_i^-)^2 + (u_i^+)^2\right) + 2\dot{u}_{ij}(\dot{u}_i^- u_i^- + \dot{u}_i^+ u_i^+) - \dot{u}_{ij}^2(u_i^- + u_i^+) - u_i^-\left(\ddot{u}_i^- u_i^- + (\dot{u}_i^-)^2\right) - u_i^+\left(\ddot{u}_i^+ u_i^+ + (\dot{u}_i^+)^2\right)\right] \\
\mu_3^v = {} & c_{301} u_{ij}(\ddot{v}_{ij} u_{ij} + 2\dot{v}_{ij}\dot{u}_{ij}) + c_{302}\dot{u}_{ij}^2 v_{ij} + c_{303} v_{ij}\left(\ddot{v}_{ij} v_{ij} + \dot{v}_{ij}^2\right) + \\
&+ c_{304}\left[v_{ij}\left((\dot{u}_j^-)^2 + (\dot{u}_j^+)^2 - 2\dot{u}_{ij}(\dot{u}_j^- + \dot{u}_j^+)\right) + 2\dot{u}_{ij}(\dot{u}_j^- v_j^- + \dot{u}_j^+ v_j^+) - \dot{u}_{ij}^2(v_j^- + v_j^+) - v_j^-(\dot{u}_j^-)^2 - v_j^+(\dot{u}_j^+)^2\right] + \\
&+ c_{305}\left[\ddot{v}_{ij}\left((u_i^-)^2 + (u_i^+)^2 - 2u_{ij}(u_i^- + u_i^+)\right) - 2\dot{v}_{ij}\left(\dot{u}_{ij}(u_i^- + u_i^+) + u_{ij}(\dot{u}_i^- + \dot{u}_i^+) - \dot{u}_i^- u_i^- - \dot{u}_i^+ u_i^+\right)\right] + \\
&- c_{305}\left[u_{ij}^2(\ddot{v}_i^- + \ddot{v}_i^+) + 2u_{ij}\left(\dot{u}_{ij}(\dot{v}_i^- + \dot{v}_i^+) - \ddot{v}_i^- u_i^- - \ddot{v}_i^+ u_i^+ - \dot{u}_i^- \dot{v}_i^- - \dot{u}_i^+ \dot{v}_i^+\right)\right] + \\
&+ c_{305}\left[2\dot{u}_{ij}(\dot{v}_i^- u_i^- + \dot{v}_i^+ u_i^+) - u_i^-(\ddot{v}_i^- u_i^- + 2\dot{u}_i^- \dot{v}_i^-) - u_i^+(\ddot{v}_i^+ u_i^+ + 2\dot{u}_i^+ \dot{v}_i^+)\right] + \\
&+ c_{306}\left[v_{ij}^2(\ddot{v}_i^- + \ddot{v}_i^+) + v_{ij}\left(2\ddot{v}_{ij}(v_i^- + v_i^+) + 2\dot{v}_{ij}(\dot{v}_i^- + \dot{v}_i^+) - 2\ddot{v}_i^- v_i^- - 2\ddot{v}_i^+ v_i^+ - (\dot{v}_i^-)^2 - (\dot{v}_i^+)^2\right)\right] + \\
&+ c_{306}\left[\dot{v}_{ij}^2(v_i^- + v_i^+) - 2\dot{v}_{ij}(\dot{v}_i^- v_i^- + \dot{v}_i^+ v_i^+) - \ddot{v}_{ij}\left((v_i^-)^2 + (v_i^+)^2\right) + v_i^-\left(\ddot{v}_i^- v_i^- + (\dot{v}_i^-)^2\right) + v_i^+\left(\ddot{v}_i^+ v_i^+ + (\dot{v}_i^+)^2\right)\right] + \\
&- c_{307}\left[u_{ij}^2(\ddot{v}_j^- + \ddot{v}_j^+) + 2u_{ij}\left(\dot{u}_{ij}(\dot{v}_j^- + \dot{v}_j^+) - \ddot{v}_j^- u_j^- - \ddot{v}_j^+ u_j^+ - \dot{u}_j^- \dot{v}_j^- - \dot{u}_j^+ \dot{v}_j^+\right) - 2\dot{u}_{ij}(\dot{v}_j^- u_j^- + \dot{v}_j^+ u_j^+)\right] + \\
&- c_{307}\left[2\dot{v}_{ij}\left(\dot{u}_{ij}(u_j^- + u_j^+) + u_{ij}(\dot{u}_j^- + \dot{u}_j^+) - \dot{u}_j^- u_j^- - \dot{u}_j^+ u_{jj}^+\right) - \ddot{u}_{ij}\left((u_j^-)^2 - 2u_{ij}(u_j^- + u_j^+) + (u_j^+)^2\right)\right] + \\
&- c_{307}\left[u_i^-(\ddot{v}_j^- u_j^- + 2\dot{u}_j^- \dot{v}_j^-) + u_j^+(\ddot{v}_j^+ u_j^+ + 2\dot{u}_j^+ \dot{v}_j^+)\right] + \\
&+ c_{308}\left[v_{ij}\left((\dot{u}_i^-)^2 - 2\dot{u}_{ij}(\dot{u}_i^- + \dot{u}_i^+) + (\dot{u}_i^+)^2\right) - \dot{u}_{ij}^2(v_i^- + v_i^+) + 2\dot{u}_{ij}(\dot{u}_i^- v_i^- + \dot{u}_i^+ v_i^+) - v_i^-(\dot{u}_i^-)^2 - v_i^+(\dot{u}_i^+)^2\right] + \\
&+ c_{309}\left[u_{ij}\left(\ddot{u}_j^- v_j^- + \ddot{u}_j^+ v_j^+ + \ddot{u}_i^- v_i^- + \ddot{u}_i^+ v_i^+ - \ddot{u}_{ij}(v_j^- + v_j^+ + v_i^- + v_i^+)\right) + \ddot{u}_{ij}(u_i^- v_i^- + u_i^+ v_i^+ + u_j^- v_j^- + u_j^+ v_j^+)\right] + \\
&+ c_{309}\left[v_{ij}\left(u_{ij}(4\ddot{u}_{ij} - \ddot{u}_i^- - \ddot{u}_i^+ - \ddot{u}_j^- - \ddot{u}_j^+) - \ddot{u}_{ij}(u_j^- + u_j^+ + u_i^- + u_i^+) + \ddot{u}_j^- u_j^- + \ddot{u}_j^+ u_j^+ + \ddot{u}_i^- u_i^- + \ddot{u}_i^+ u_i^+\right)\right] + \\
&- c_{309}\left[\ddot{u}_j^- u_j^- v_j^- + \ddot{u}_j^+ u_j^+ v_j^+ + \ddot{u}_i^- u_i^- v_i^- + \ddot{u}_i^+ u_i^+ v_i^+\right] + \\
&- c_{310}\left[v_{ij}^2(\ddot{v}_j^- + \ddot{v}_j^+) + v_{ij}\left(2\ddot{v}_{ij}(v_j^- + v_j^+) + 2\dot{v}_{ij}(\dot{v}_j^- + \dot{v}_j^+) - 2\ddot{v}_j^- v_j^- - 2\ddot{v}_j^+ v_j^+ - (\dot{v}_j^-)^2 - (\dot{v}_j^+)^2\right)\right] + \\
&+ c_{310}\left[\ddot{v}_{ij}\left((v_j^-)^2 + (v_j^+)^2\right) + 2\dot{v}_{ij}(\dot{v}_j^- v_j^- + \dot{v}_j^+ v_j^+) - \dot{v}_{ij}^2(v_j^- + v_j^+) - v_j^-\left(\ddot{v}_j^- v_j^- + (\dot{v}_j^-)^2\right) - v_j^+\left(\ddot{v}_j^+ v_j^+ + (\dot{v}_j^+)^2\right)\right]
\end{aligned}
\tag{A.8}
$$

where the nonlinear quadratic coefficients are

$$
\begin{aligned}
c_{21} &= \tfrac{1}{2}\varrho^2 \csc^2(\alpha) \\
c_{22} &= \tfrac{1}{2}\varrho^2 \cot^2(\alpha)\csc^2(\alpha) \\
c_{23} &= 2\varrho^2 \cot(2\alpha)\csc(2\alpha) \\
c_{24} &= \varrho^2 \sec^2(\alpha)
\end{aligned}
\tag{A.9}
$$

and the nonlinear cubic coefficients are

$$
\begin{aligned}
c_{301} &= \tfrac{1}{4}\varrho^2\left(7 - 6\cos(2\alpha) + 3\cos(4\alpha)\right)\csc^4(\alpha)\sec^2(\alpha) \\
c_{302} &= \tfrac{1}{4}\varrho^2\left(7 + 2\cos(2\alpha) + 3\cos(4\alpha)\right)\csc^4(\alpha)\sec^2(\alpha) \\
c_{303} &= \tfrac{1}{16}\varrho^2\left(45\cos(2\alpha) + 4\cos(4\alpha) + 3(4 + \cos(6\alpha))\right)\csc^6(\alpha)\sec^2(\alpha) \\
c_{304} &= \tfrac{1}{4}\varrho^2\left(1 + 3\cos(2\alpha)\right)\csc^4(\alpha) \\
c_{305} &= \tfrac{3}{2}\varrho^2 \sec^2(\alpha) \\
c_{306} &= \tfrac{1}{4}\varrho^2\left(1 - 3\cos(2\alpha)\right)\csc^2(\alpha)\sec^2(\alpha) \\
c_{307} &= \tfrac{1}{16}\varrho^2\left(5 + 3\cos(4\alpha)\right)\csc^4(\alpha)\sec^2(\alpha) \\
c_{308} &= \tfrac{1}{16}\varrho^2\left(9 - 4\cos(2\alpha) + 3\cos(4\alpha)\right)\csc^4(\alpha)\sec^2(\alpha) \\
c_{309} &= \tfrac{1}{8}\varrho^2\left(7 - 2\cos(2\alpha) + 3\cos(4\alpha)\right)\csc^4(\alpha)\sec^2(\alpha) \\
c_{310} &= \tfrac{1}{2}\varrho^2 \cot^4(\alpha)\csc^2(\alpha)\left(3 + \sec^2(\alpha)\right).
\end{aligned}
\tag{A.10}
$$

Appendix B. Nonlinear dispersion relation

The matrices and operators governing the third order pair of nonlinear eigenproblems (18), (19) read

$$
\mathbf{F}_1 = \begin{bmatrix} F_{1aa} & 0 \\ 0 & F_{1cc} \end{bmatrix}, \qquad \mathbf{G}_1 = \begin{bmatrix} G_{1aa} & 0 \\ 0 & G_{1cc} \end{bmatrix}, \qquad \mathbf{F}_3 = \begin{bmatrix} F_{3aa} & F_{3ac} \\ F_{3ca} & F_{3cc} \end{bmatrix}, \qquad \mathbf{G}_3 = \begin{bmatrix} G_{3aa} & G_{3ac} \\ G_{3ca} & G_{3cc} \end{bmatrix},
\tag{B.1}
$$

where the coefficients are

$$
\begin{aligned}
F_{1aa} &= 4\Psi_1 \\
F_{1cc} &= 2\Psi_2 \\
G_{1aa} &= 2 + 2\varrho^2\left(2\Psi_0 + \csc^2(\alpha)\Psi_1 + \sec^2(\alpha)\Psi_2\right) \\
G_{1cc} &= 2 + 2\varrho^2\left(2\Psi_0 + \csc^2(\alpha)\Psi_2 + \sec^2(\alpha)\Psi_1\right) \\
F_{3aa} &= 12\Psi_2^2\left(a_1^2 + b_1^2\right) - 8\Psi_5^2\left(3c_1^2 + d_1^2\right) \\
F_{3cc} &= 12\Psi_1^2\left(c_1^2 + d_1^2\right) - 8\Psi_5^2\left(3a_1^2 + b_1^2\right) \\
F_{3ac} &= -16\Psi_5^2 b_1 d_1 \\
G_{3aa} &= 8\varrho^2\sec^2(\alpha)\left[\Psi_5^2\left(5c_1^2 + 3d_1^2\right) - 2\Psi_2^2\left(a_1^2 + b_1^2\right)\right] - 8\varrho^2\csc^2(\alpha)\left[4\Psi_5^2 c_1^2 - \Psi_6^2\left(a_1^2 + b_1^2\right)\right] + \\
&\quad + 4\varrho^2\csc^4(\alpha)\left[\Psi_5^2\left(5c_1^2 - d_1^2\right) - 14\Psi_1^2\left(a_1^2 + b_1^2\right)\right] + 32\varrho^2\Psi_1^2\csc^6(\alpha)\left(a_1^2 + b_1^2\right) \\
G_{3cc} &= 8\varrho^2\sec^2(\alpha)\left[\Psi_5^2\left(5a_1^2 + 3b_1^2\right) 2\Psi_1^2\left(c_1^2 + d_1^2\right)\right] - 8\varrho^2\csc^2(\alpha)\left[4\Psi_5^2 a_1^2 - \Psi_7\left(c_1^2 + d_1^2\right)\right] + \\
&\quad + 4\varrho^2\csc^4(\alpha)\left[\Psi_5^2\left(5a_1^2 - b_1^2\right) - 14\Psi_2^2\left(c_1^2 + d_1^2\right)\right] + 32\varrho^2\Psi_2^2\csc^6(\alpha)\left(c_1^2 + d_1^2\right) \\
G_{3ac} &= 2\varrho^2\csc^4(\alpha)\sec^2(\alpha)\left[7 + 2\cos(2\alpha) + 3\cos(4\alpha)\right]\Psi_5^2 b_1 d_1
\end{aligned}
\tag{B.2}
$$

and the auxiliary quantities $\Psi_0 = \cos\beta_1 + \cos\beta_2$, $\Psi_1 = 1 - \cos\beta_1$, $\Psi_2 = 1 - \cos\beta_2$, $\Psi_3^2 = \cos\beta_1(2 - \cos\beta_1)$, $\Psi_4^2 = \cos\beta_2(2 - \cos\beta_2)$, $\Psi_5^2 = 2 - \Psi_3^2 - \Psi_4^2$, $\Psi_6^2 = 4 - 3\Psi_3^2 - \Psi_4^2$, $\Psi_7^2 = 4 - \Psi_3^2 - 3\Psi_4^2$ have been introduced.

Data availability

Data will be made available on request.

References

[1] F. Romeo, M. Ruzzene, Wave Propagation in Linear and Nonlinear Periodic Media: Analysis and Applications, vol. 540, Springer Science & Business Media, 2013.
[2] M.I. Hussein, M.J. Leamy, M. Ruzzene, Dynamics of phononic materials and structures: historical origins, recent progress, and future outlook, Appl. Mech. Rev. 66 (4) (2014) 040802.
[3] M.A. Porter, P.G. Kevrekidis, C. Daraio, Granular crystals: nonlinear dynamics meets materials engineering, Phys. Today 68 (11) (2015) 44–50.
[4] G.U. Patil, K.H. Matlack, Review of exploiting nonlinearity in phononic materials to enable nonlinear wave responses, Acta Mech. 233 (1) (2022) 1–46.
[5] M.D. Fronk, L. Fang, P. Packo, M.J. Leamy, Elastic wave propagation in weakly nonlinear media and metamaterials: a review of recent developments, Nonlinear Dyn. 111 (12) (2023) 10709–10741.
[6] V. Laude, Principles and properties of phononic crystal waveguides, APL Mater. 9 (8) (2021) 080701.
[7] P. Jiao, J. Mueller, J.R. Raney, X. Zheng, A.H. Alavi, Mechanical metamaterials and beyond, Nat. Commun. 14 (2023) 6004.
[8] A. Krushynska, D. Torrent, A.M. Aragón, et al., Emerging topics in nanophononics and elastic, acoustic, and mechanical metamaterials: an overview, Nanophotonics 12 (4) (2023) 659–686.
[9] M. Kadic, T. Bückmann, R. Schittny, M. Wegener, Metamaterials beyond electromagnetism, Rep. Prog. Phys. 76 (12) (2013) 126501.
[10] J. Ma, Phonon engineering of micro- and nanophononic crystals and acoustic metamaterials: a review, Small Sci. 3 (1) (2023) 2200052.
[11] J. Zhang, B. Hu, S. Wang, Review and perspective on acoustic metamaterials: from fundamentals to applications, Appl. Phys. Lett. 123 (1) (2023) 010502.
[12] X. Fang, W. Lacarbonara, L. Cheng, Advances in nonlinear acoustic/elastic metamaterials and metastructures, Nonlinear Dyn. (2024), https://doi.org/10.1007/s11071-024-10219-4.
[13] C. Yilmaz, G.M. Hulbert, N. Kikuchi, Phononic band gaps induced by inertial amplification in periodic media, Phys. Rev. B 76 (5) (2007) 054309.
[14] M. Barys, J.S. Jensen, N.M. Frandsen, Efficient attenuation of beam vibrations by inertial amplification, Eur. J. Mech. A, Solids 71 (2018) 245–257.
[15] S. Muhammad, S. Wang, F. Li, C. Zhang, Bandgap enhancement of periodic nonuniform metamaterial beams with inertial amplification mechanisms, J. Vib. Control 26 (15–16) (2020) 1309–1318.
[16] O. Yuksel, C. Yilmaz, Realization of an ultrawide stop band in a 2-d elastic metamaterial with topologically optimized inertial amplification mechanisms, Int. J. Solids Struct. 203 (2020) 138–150.
[17] N.M. Frandsen, O.R. Bilal, J.S. Jensen, M.I. Hussein, Inertial amplification of continuous structures: large band gaps from small masses, J. Appl. Phys. 119 (12) (2016) 124902.
[18] A. Banerjee, S. Adhikari, M.I. Hussein, Inertial amplification band-gap generation by coupling a levered mass with a locally resonant mass, Int. J. Mech. Sci. 207 (2021) 106630.
[19] M.I. Hussein, I. Patrick, A. Banerjee, S. Adhikari, Metadamping in inertially amplified metamaterials: trade-off between spatial attenuation and temporal attenuation, J. Sound Vib. 531 (2022) 116977.
[20] V. Settimi, M. Lepidi, A. Bacigalupo, Analytical spectral design of mechanical metamaterials with inertia amplification, Eng. Struct. 274 (2023) 115054.
[21] V. Settimi, M. Lepidi, A. Bacigalupo, Nonlinear dispersion properties of one-dimensional mechanical metamaterials with inertia amplification, Int. J. Mech. Sci. 201 (2021) 106461.
[22] M. Lepidi, V. Settimi, Harmonic and superharmonic components in periodic waves propagating through mechanical metamaterials with inertial amplification, in: W. Lacarbonara (Ed.), Advances in Nonlinear Dynamics, Volume III, Springer Nature Switzerland, Cham, 2024, pp. 541–551.
[23] B.S. Lazarov, J.S. Jensen, Low-frequency band gaps in chains with attached non-linear oscillators, Int. J. Non-Linear Mech. 42 (10) (2007) 1186–1193.
[24] R.K. Narisetti, M. Ruzzene, M.J. Leamy, Study of wave propagation in strongly nonlinear periodic lattices using a harmonic balance approach, Wave Motion 49 (2) (2012) 394–410.
[25] R.K. Narisetti, M.J. Leamy, M. Ruzzene, A perturbation approach for predicting wave propagation in one-dimensional nonlinear periodic structures, J. Vib. Acoust. 132 (3) (2010) 031001.

[26] R.K. Narisetti, M. Ruzzene, M.J. Leamy, A perturbation approach for analyzing dispersion and group velocities in two-dimensional nonlinear periodic lattices, J. Vib. Acoust. 133 (6) (2011) 061020.
[27] M.-A. Campana, M. Ouisse, E. Sadoulet-Reboul, M. Ruzzene, S. Neild, F. Scarpa, Impact of non-linear resonators in periodic structures using a perturbation approach, Mech. Syst. Signal Process. 135 (2020) 106408.
[28] Z. Chen, W. Zhou, C. Lim, Active control for acoustic wave propagation in nonlinear diatomic acoustic metamaterials, Int. J. Non-Linear Mech. 125 (2020) 103535.
[29] A.F. Vakakis, M.E. King, Nonlinear wave transmission in a monocoupled elastic periodic system, J. Acoust. Soc. Am. 98 (3) (1995) 1534–1546.
[30] K. Manktelow, M.J. Leamy, M. Ruzzene, Multiple scales analysis of wave–wave interactions in a cubically nonlinear monoatomic chain, Nonlinear Dyn. 63 (1–2) (2011) 193–203.
[31] M. Lepidi, A. Bacigalupo, Wave propagation properties of one-dimensional acoustic metamaterials with nonlinear diatomic microstructure, Nonlinear Dyn. 98 (4) (2019) 2711–2735.
[32] Y. Shen, W. Lacarbonara, Nonlinearity enhanced wave bandgaps in metamaterial honeycombs embedding spider web-like resonators, J. Sound Vib. (2023) 117821.
[33] L. Fang, M.J. Leamy, A perturbation approach for predicting wave propagation at the spatial interface of linear and nonlinear one-dimensional lattice structures, Nonlinear Dyn. 112 (2024) 5015–5036.
[34] A. Fortunati, A. Bacigalupo, M. Lepidi, A. Arena, W. Lacarbonara, Nonlinear wave propagation in locally dissipative metamaterials via Hamiltonian perturbation approach, Nonlinear Dyn. 108 (2) (2022) 765–787.
[35] A. Fortunati, A. Arena, M. Lepidi, A. Bacigalupo, W. Lacarbonara, Free propagation of resonant waves in nonlinear dissipative metamaterials, Proc. R. Soc. A, Math. Phys. Eng. Sci. 480 (2024) 20230759.
[36] A. Bacigalupo, M. Lepidi, Acoustic wave polarization and energy flow in periodic beam lattice materials, Int. J. Solids Struct. 147 (2018) 183–203.
[37] M. Thorpe, Bulk and surface floppy modes, J. Non-Cryst. Solids 182 (1–2) (1995) 135–142.
[38] A.P. Giddy, M.T. Dove, G.S. Pawley, V. Heine, The determination of rigid-unit modes as potential soft modes for displacive phase transitions in framework crystal structures, Acta Crystallogr., Sect. A, Found. Crystallogr. 49 (5) (1993) 697–703.
[39] M.D. Fronk, M.J. Leamy, Internally resonant wave energy exchange in weakly nonlinear lattices and metamaterials, Phys. Rev. E 100 (3) (2019) 032213.
[40] W. Jiao, S. Gonella, Intermodal and subwavelength energy trapping in nonlinear metamaterial waveguides, Phys. Rev. Appl. 10 (2) (2018) 024006.
[41] M. Lepidi, Multi-parameter perturbation methods for the eigensolution sensitivity analysis of nearly-resonant non-defective multi-degree-of-freedom systems, J. Sound Vib. 332 (4) (2013) 1011–1032.
[42] A. Bacigalupo, M. Lepidi, High-frequency parametric approximation of the Floquet-Bloch spectrum for anti-tetrachiral materials, Int. J. Solids Struct. 97–98 (2016) 575–592.
[43] W. Lacarbonara, R. Camillacci, Nonlinear normal modes of structural systems via asymptotic approach, Int. J. Solids Struct. 41 (20) (2004) 5565–5594.
[44] H. Ding, L.-Q. Chen, Designs, analysis, and applications of nonlinear energy sinks, Nonlinear Dyn. 100 (4) (2020) 3061–3107.